UNIVERSIDADE D
COIMBRA

Eduardo Celso Cruz Monteiro

MECHANICAL CHARACTERIZATION OF CEMENT AND GYPSUM BASED MORTARS WITH NANO AND MICRO SILICA PARTICLES FOR PASSIVE FIRE PROTECTION OF STEEL STRUCTURES

Master's Dissertation in Civil Engineering, in the Specialization area in Structural Mechanics, under the scientific advising of Prof. Doctor Aldina Maria da Cruz Santiago and Doctor Hugo Filipe dos Santos Caetano, presented to the Civil Engineering Department of the Faculty of Science and Technology of the University of Coimbra

July of 2022

Faculty of Sciences and Technology of the University of Coimbra
Department of Civil Engineering

Eduardo Celso Cruz Monteiro

MECHANICAL CHARACTERIZATION OF CEMENT AND GYPSUM BASED MORTARS WITH NANO AND MICRO SILICA PARTICLES FOR PASSIVE FIRE PROTECTION OF STEEL STRUCTURES

CARACTERIZAÇÃO MECÂNICA DE ARGAMASSAS DE PROTEÇÃO PASSIVA AO FOGO EM ESTRUTURAS METÁLICAS DE BASE CIMENTÍCIA E GESSO COM PARTÍCULAS DE NANO E MICRO SÍLICA

Master's Dissertation in Civil Engineering, in the Specialization area in Structural Mechanics, under the scientific advising of Prof. Doctor Aldina Maria da Cruz Santiago and Doctor Hugo Filipe dos Santos Caetano, presented to the Civil Engineering Department of the Faculty of Science and Technology of the University of Coimbra.

July of 2022

1 2 9 0

UNIVERSIDADE D
COIMBRA

In memoriam of my grandmother,
Maria do Socorro Cruz.

ACKNOWLEDGEMENTS

I'm thankful to Jesus, my King, because nothing would be possible without You. Your greatness, kindness and provision took me here and will guide me forth. For Psalm 23:1 "The Lord is my shepherd; I shall not want" and Matthew 11:30 "For my yoke is good, and the weight I take up is not hard", thank You.

I'm thankful to my parents, who did not measure efforts to bring me to Portugal. Indeed, it's needed so much love to let a son leave the country, and so I hope I could honour you, Afonso Monteiro and Kátia Monteiro. Your support and love were, are and always will be fundamental in my life. Also to my brother Olavo Monteiro, my family and my sister Daniela Monteiro who always gave me support and love. Your life is essential to mine. I'm thankful to my girlfriend, Bianca Botaro, who has been a gift in my life. I'm thankful for all my colleagues, especially João Campana and Caio Battaglia, who have always been with me, helping each other. I'm thankful for the love and life of my grandmother, Maria do Socorro Cruz, who was the bravest person I know. We couldn't say goodbye, so I dedicated this work to you. Love you for eternity.

I'm thankful for the assistance provided by all Professors and employees from DEC, to all my friends who accompanied me here and to Extrema Church.

Special acknowledgements are addressed to Professors Doctors Aldina Santiago, Hugo Caetano and Luís Laim for providing me with the opportunity of integrating the NanoFire project and for the assistance and friendship during this last year. I'm grateful for the assistance given by Professors Doctors Almicar Ramalho and Luis Vilhena, António Lopes, Lígia Abreu and all the staff of the LEMEC/FCTUC.

This dissertation was supported by the Portuguese Foundation for Science and Technology (FCT) for its support under the framework of research project PTDC/ECI-EGC/31850/2017 (NANOFIRE—Thermal and Mechanical behaviour of Nano Cements and their application in steel construction as fire protection), to the University of Coimbra (UC), and was also financed by FEDER funds through the Competitivity Factors Operational Programme—COMPETE and by national funds through FCT within the scope of the project POCI-01-0145-FEDER-007633 and through the Regional Operational Programme CENTRO2020 within the scope of the project CENTRO-01-0145-FEDER-000006.

ABSTRACT

Steel structures are worldwide used in several civil engineering projects for their wide range of benefits such as: easy modelling, assembly and disassembly, reduced time of construction, reuse versatility, type of green construction, and high capacity resist to considerable loads while having a reduced weight. However, as the temperature grows, the steel's mechanical properties suffer a softening process under a fire. These reductions tend to be more expressive from 500 ºC, usually considered the structural steel's critical temperature. Therefore, to safeguard the steel structure's partial and global stability and preserve the existing goods and its users' lives, passive protection measures are required to ensure the safety levels required by structural regulations.

In this context, the main objective of this dissertation was the development and the mechanical characterization of cement and gypsum based passive fire protection mortars with nano and micro silica (NMS) particles. The mortars were constituted by different materials such as vermiculite, perlite, polypropylene fibres and NMS particles. The mortars` mechanical characterization will be carried out through non-destructive and destructive tests. The non-destructive tests proceeding included the determination of the Young's modulus, shear modulus and Poisson's ratio, and through the destructive tests, the flexural and the compression strengths of each mortar composition were determined. Moreover, TGA, XRD and SEM were carried out as complementary tests.

The experimental work was part of the research project NanoFire: Thermal and Mechanical behaviour of Nano Cements and their application in steel construction as fire protection, currently in progress at the University of Coimbra.

Keywords: cement and gypsum based mortars, mechanical characterization, passive fire protection, steel structures, vermiculite, perlite and polypropylene fibres.

RESUMO

As estruturas metálicas são utilizadas em diversos tipos de projetos de engenharia civil à escala global devido ao grande número de benefícios que estas oferecem, tais como: facilidade de modelação, montagem e desmontagem, tempos reduzidos de construção, versatilidade de reutilização, tipo de construção sustentável e elevada capacidade para suportar esforços consideráveis com um peso próprio reduzido. No entanto, em situação de incêndio, as propriedades mecânicas do aço vão sendo reduzidas à medida a que a temperatura vai aumentando e, a partir dos 500 ºC, considerada normalmente como temperatura crítica do aço estrutural, estas reduções mecânicas são mais significativas. Portanto, para salvaguardar a estabilidade parcial e global de uma estrutura metálica, preservar os bens existentes e salvaguardar a vida dos seus ocupantes, é fundamental a adoção de medidas de proteção passiva que garantam os níveis de segurança exigidos pelos regulamentos estruturais.

O objetivo principal do trabalho desta dissertação foi o desenvolvimento e a caracterização mecânica de diferentes argamassas de proteção passiva contra o fogo à base de gesso ou cimento com a adição de micro e nano partículas de sílica (NMS). Estas argamassas foram constituídas por diversos materiais, tais como vermiculite, perlite, fibras de polipropileno e partículas de NMS. A caracterização mecânica das argamassas foi realizada através de ensaios não destrutivos e destrutivos. Os ensaios não destrutivos englobaram a determinação dos módulos de Young, módulos de elasticidade transversal e coeficientes de Poisson e, através de ensaios destrutivos sforam determinadas as resistências à compressão e à flexão de cada argamassa. Além disso, também foram realizados testes TGA, XRD e SEM, definidos como testes complementares.

O trabalho experimental enquadrou-se na execução do projeto NanoFire: Comportamento térmico e mecânico de Nano Cimentos e sua aplicação na construção de aço como revestimento de proteção passiva contra incêndios, atualmente em curso na Universidade de Coimbra.

Palavras-chave: argamassas à base de gesso e cimento, caracterização mecânica, proteção passiva ao fogo, estruturas metálicas, vermiculite, perlite e fibras de polipropileno.

TABLE OF CONTENTS

FIGURE INDEX

TABLE INDEX

NOTATIONS

θ_a	The steel temperature
ρ	Density
μ	Poisson's ratio
vs	Versus
$f_{ct,c}$	Compression strength
$f_{ct,fl}$	Flexural strength
f_f	Fundamental resonant frequency of bar in flexure
ft	Fundamental resonant frequency of bar in torsion
Vp	Pulse-propagation velocity of the compression wave
Vs	Pulse-propagation velocity of the shear wave

ABBREVIATIONS

AFP	Active fire protection
C	Commercial passive protection solution used as reference mortar
Ca^{2+}	Calcium ion
$Ca_6Al_2(SO_4)_3(OH)_{12}\cdot 26H_2O$	Calcium sulfoaluminate hydrate
$CaCO_3$	Calcium carbonate (calcite)
$CaSO_4$	Calcium sulfate (anhydrite)
$CaSO_4 \cdot 2H_2O$	Calcium sulfate di-hydrate (Gypsum)
$CaSO_4 \cdot 0.5H_2O$	Calcium sulfate hemihydrate
CH	Calcium hydroxide
CO_2	Carbon dioxide
CPPS	Commercial passive protection solution
CP	Compression
C-S-H	Calcium silicate hydrate
CV	Developed cement mortar with vermiculite and polypropylene fibres
CV.NMS	Developed cement mortar with vermiculite and polypropylene fibres, nano and micro silica particles
E	Young's modulus
EP	Expanded perlite
EV	Expanded vermiculite
FL	Flexural
G	Shear modulus
GP	Developed gypsum mortar with perlite
GP.NMS	Developed gypsum mortar with perlite, nano and micro silica particles
GV	Developed gypsum mortar with vermiculite
GV.NMS	Developed gypsum mortar with vermiculite, nano and micro silica particles
GY	Gypsum powder
IEV	Impulse excitation of vibration
MS	Microparticles of silica
nano-Al_2O_3	Aluminium Oxide Nanoparticles
nano-Fe_2O_3	Iron Oxide Nanoparticles

nano-SiO_2	Silicon Oxide Nanoparticles
NMS	Nano and microparticles of silica
NS	Nanoparticles of silica
PC	Portland cement CEM II/B-L 32.5
PFP	Passive fire protection
PP	Polypropylene fibres
Ref.	Reference
RH	Relative humidity
SD	Standard deviation
SEM	Scanning electron microscopy
SiO_2	Silicon dioxide
TGA	Thermo gravimetric analysis
ULS	Ultimate limit state
UPV	Ultrasonic pulse velocity
V/B	Vermiculite to binder ratio
W	Water
W/B	Water to binder ratio in weight %
XRD	X-ray diffraction

1 INTRODUCTION

1.1 Initial considerations

The present work is within the scope of the national research project PTDC/ECI-EGC/31850/2017 (NANOFIRE - Thermal and Mechanical behaviour of Nano Cements and their application in steel construction as fire protection), funded by FCT (Foundation for Science and Technology). The project's main objective is to develop mortars with nano particles, to enhance its behaviour under fire situations as passive fire protection material for steel structures.

The author was involved in different types of activities such as: i) the preparation of the specimens and their physical characterization and experimental mechanical characterization tests, ii) the treatment of the data, iii) the elaboration of the state-of-the-art review and iv) the assistance on the scientific research report writing. Moreover, the author also collaborated on the complementary tests carried out at IPN (Pedro Nunes Institute), based in Coimbra - Portugal.

Finally, the author also contributed to other activities in the scope of the project which were not part of this dissertation: i) fabrication and preparation of different passive fire protection mortars in SHS columns, ii) evaluation of the fire resistance of steel columns under axial loading, protected with different fire protection mortars through experimental tests and iii) fabrication and preparation of specimens to obtain a patent.

1.2 Overview

Widely used in structural design for their many valuable benefits, such as its strength to weight ratio, ductility, fast construction and sustainability, steel sections are nonetheless highly vulnerable to fire [1-4]. When heated, steel undergoes a rapid degradation of strength and elastic modulus, which may lead to a fast and uncontrolled collapse. Therefore, it usually need to be protected by a fire protection system to ensure human safety, reduce material loss and comply with existing standards [5,6]. In the general context of fire safety, the critical temperature for such members is generally regarded to 500 ºC; in other words, it is the range of temperature at which structural steel’s design resistance equals the design effect of accidental actions [7-10].

Fire protection systems are divided into active and passive fire protection materials or methods. Active fire protection (AFP) devices detect and work to extinguish the fire [10-12], while passive fire protection (PFP) works to ensure structural stability until the fire is controlled or extinguished [10, 13-15]. The most common AFP solutions are fire extinguishers, fire hose reels, sprinkler systems, smoke alarms and firefighters. Concerning the PFPs, methods such as fire-resistant borders, intumescent paints, insulation paints and fire-protecting mortars are highly used and studied. Compared to PFP methods, AFPs are more efficient but usually more expensive. According to Milke (2015) [16], fire protection engineers assess the nature and magnitude of fire and the selection of the strategies above-mentioned.

When protection consists of positioning another material between the steel and the fire, the material and its quantity should be chosen carefully. According to EN 1993-1-2 [17], the heating rate of the steel members depends, beyond the fire's characteristics, upon the material's surface/volume ratio and its thermal and mechanical behaviour. This is explained by: i) heat is transferred from molecule to molecule in this case; therefore, heat spread is decreased as the material's contact area reduces and its thickness increases; ii) thermal conductivity, specific heat, and specific weight directly affect the heat transfer process as the velocity of heating is directly proportional to the first and inversely proportional to the specific heat and weight; and iii) the material has to resist both thermal and displacement actions, as much as possible, to ensure the stability and homogeneity needed to perform its expected insulating function during the fire event.

In the case of this study, passive fire protection mortar is highly used in steel structures, mostly when the aesthetic aspect isn't a requirement, as it ensures the stability of the structure with a reduced investment of financial resources compared to other methods [18].

1.3 Research objectives and scopes

This work presents the results of experimental research work to characterize the mechanical properties of cement and gypsum based with nano and micro silica particles passive fire protection mortars by destructive and non-destructive tests.

From previous Nanofire research [19], it was selected a group of compositions with the best thermal behaviour. Different contents of polypropylene fibre, expanded perlite, expanded vermiculite and nano and micro silica particles were used in the compositions. One composition has been studied, a commercial solution (C), as reference composition, and six others have been developed in the laboratory: i) one cement based composition with expanded vermiculite and polypropylene fibre (CV); ii) two gypsum based compositions with perlite (GP) or vermiculite

(GV), and iii) three compositions but with the addition of nano and micro silica particles (CV.NMS, GP.NMS and GV.NMS).

A total of twenty-eight 160 x 40 x 40 mm specimens were carried out by ultrasonic pulse velocity test, flexural and compression tests, and seven 200 x 100 x 40 mm specimens were carried out by impulse excitation of vibration test. By non-destructive tests, the Young's modulus (E), shear modulus (G) and Poisson's ratio (μ) were assessed, while the flexural and compression strengths were assessed by destructive tests. Moreover, density and porosity tests, Thermogravimetric Analysis (TGA), X-Ray Diffraction (XRD) and Scanning Electron Microscopy (SEM) were carried out. Lastly, the properties results were assessed and compared with literature values.

1.4 Contents of the Dissertation

The present work is organized into five chapters:

Chapter One is the introduction of the dissertation, where the overview, scopes and objectives are presented, aiming to summarize, succinctly, the content of the project and the work where developed.

Chapter Two justifies the use and development of passive fire protection mortars for steel structures and a state-of-the-art review of the materials and PPF cement and gypsum based mortars.

Chapter Three presents the studied mortars' compositions, their fabrication process, the experimental testing systems, and the procedure carried out for the mechanical characterization of the mortars.

Chapter Four presents the procedure and the results of the complementary tests, the results of the non-destructive and destructive tests, followed by a discussion based on the literature review.

Finally, Chapter Five brings the work's conclusions and the proposed future works.

2 LITERATURE REVIEW

2.1 Theoretical and normative framework of the research study

Standard design methods and rules for the different types of structures have been a concern on the past years. With that objective and under the guidance of CEN Technical Committee 250 (CEN/TC250), the EN Eurocodes have been developed and are divided into ten parts:

1. EN 1990, Eurocode 0: Basis of structural design;
2. EN 1991, Eurocode 1: Actions on structures;
3. EN 1992, Eurocode 2: Design of concrete structures;
4. EN 1993, Eurocode 3: Design of steel structures;
5. EN 1994, Eurocode 4: Design of composite steel and concrete structures;
6. EN 1995, Eurocode 5: Design of timber structures;
7. EN 1996, Eurocode 6: Design of masonry structures;
8. EN 1997, Eurocode 7: Geotechnical design;
9. EN 1998, Eurocode 8: Design of structures for earthquake resistance;
10. EN 1999, Eurocode 9: Design of aluminium structures.

Normalized by EN 19931-1 [20], steel design is under several variables' conditions, however, some moulds its baselines. Among them, selecting the most efficient steel's yield stress is one of the most important prerequisites for the economical design of this type of construction [21]. The 275 and 355 MPa steel grades are most commonly used in Portugal. However, a decrease in the difficulties associated with manufacturing steel materials [22-23] and increased demand for new steel with enhanced structural behaviour have been observed. Three new families of steels are arising: i) high strength steels (HSS), with a yield stress of 460 to 560 MPa, ii) ultra-high strength steels (HPS), featuring yield stress above 560 MPa and iii) high-performance steels which are HSS and HPS but with exceptional technological features. Therefore, the designer shall pay attention to the selection of the steel's yield stress as the relative cost of the material decreases as the strength increases [24].

However, experimental studies show that, under high temperature, steel's mechanical properties suffer a softening process due to the reduction of its yield stress, proportional limit and Young's modulus [25-28]. Thus, it's fundamental to understand the behaviour of the steel under a fire situation to proceed with the selection, or not, of the protective materials and/or methods [29].

Each of the codes, except for EN 1990 [30], is divided into parts. In Portugal, the structural fire design of steel structures is normalized in EN 1993 part 1-2, and has to comply with the exposed in Decree Law n.º 220/2008 [31] and Ministerial Orders n.º 1532/2008 [32] and actual corresponding versions. Complying the requeriments, the structure is classified with a minimum value of fire resistance to provide structural support (R), watertightness (E) and/or thermal insulation (I). Each function has to resist from 30 to 180 minutes, according to the risk in consideration.

According to the above-mentioned Eurocode, the variation of the steel's yield stress, proportional limit and Young's modulus is dependent of temperature in accordance with the reduction factors (RF) [33] given in Table 2.1. In the same table, it is possible to compare the reduction factors' values with the steel temperature (θ_a).

Table 2.1 - Reduction factors, relative to the values of f_y and E_a at 20 ºC, for the stress-strain relationship of carbon steel at high temperatures and a comparison between RFs with the increasing of 100 ºC of the steel temperature (adapted from Ref. [17]).

Temperature	**RF**	**Ratio (%)**	**RF**	**Ratio (%)**	**RF**	**Ratio (%)**
θ_a (ºC)	**$k_{y,\theta}= f_{y,\theta}/f_y$**	**$k_{y,\theta}/ k_{y,\theta-100}$**	**$k_{p,\theta}= f_{y,\theta}/f_y$**	**$k_{p,\theta}/ k_{p,\theta-100}$**	**$k_{E,\theta}= E_{a,\theta}/E_a$**	**$k_{E,\theta}/ k_{E,\theta-100}$**
100	1.00	100	1.00	100	1.00	100
200	1.00	100	0.81	81	0.90	90
300	1.00	100	0.61	76	0.80	89
400	1.00	100	0.42	69	0.70	88
500	0.78	78	0.36	86	0.60	86
600	0.47	60	0.18	50	0.31	52
700	0.23	49	0.08	42	0.13	42
800	0.11	48	0.05	67	0.09	69
900	0.06	55	0.038	75	0.068	75
1000	0.04	67	0.025	67	0.045	67
1100	0.02	50	0.013	50	0.023	50
1200	0.00	0	0.00	0	0.000	0

The assessment of Table 2.1 allowed a clear picture of the decrease of the mechanical properties' values from 400 to 600 ºC, in comparison to the ambient temperature's values. At 600 ºC, a drop of 40%, 50% and 48% from the 500 ºC's yield stress, proportional limit and Young's modulus values is observed. It endorses the disposed in Ref. [5-10], concerning the critical temperature in the range of 500 ºC. Therefore, in most cases, it's essential to protect the steel with a protection measure to delay the heat increasing and guarantee the safety required [34-35].

2.2 Passive fire protection methods

According to Ref. [35], the construction works must be designed and build in such a way, that in the event of an outbreak of fire, the load bearing resistance of the construction can be assumed for a specified period of time, the generation and spread of fire and smoke within the works are limited, the spread of fire to neighbouring construction works is limited, the occupants can leave the works or can be rescued by other means and the safety of rescue teams is taken into consideration. In this context, passive fire protection systems control the spread of fire and prevent or delay the collapse of compartments [10, 34].

The material selection shall attend to the fire safety requirements; however, the aesthetic requirement is also an important step to comply with. Currently, the intumescent paintings are the passive fire protection method that best fits this requirement [18, 36].

At ambient temperature, paintings are inert however they can expand and degrade at temperatures of 280 to 350 ºC, to provide a layer of low conductivity materials, which acts as a heat transfer barrier to protect the coated structure, physically and thermally [37]. This method presents other strengths, such as reduced weight and waste, provides a high-quality finishing, and it's indicated to complex shapes [38]. The main disadvantage is the price compared to sprayed solutions [39]. For example, in Portugal, the cost is 15 to 20 euros per m^2 [40] and demands specialized manpower, which increases the expenses. The solution is represented in Figure 2.1.

(a) **(b)** **(c)**

Figure 2.1 – Intumescent painting in different phases: specialized application procedure (a), under proceeding (b) and under high temperature at its expanded form (c) (from Ref. [41-43], respectively).

On the opposite side of the intumescent paintings, the flexible blanket system is one of the cheapest solutions [44]. This solution presents a reduced thermal conductivity, mainly composed of rock or glass wool. Also, it allows a clean installation procedure and is a lightweight material. The main disadvantage is its aesthetical appearance [39]. The solution is shown in Figure 2.2.

(a) **(b)** **(c)**

Figure 2.2 – Flexible blanket systems: rock wool (a), glass wool under installation procedure (b) and beams coated by the material (c) (from Ref. [45, 46 and 39], respectively).

A very commonly used method is the intumescent board systems. It is widely used due to its ease of manufacture, widespread availability of the materials for its production, environmental friendliness, and energy-consuming dehydration process [47]. The mainly used materials to manufacture the boards are gypsum, cement, vermiculite and perlite [37]. Also, it guarantees a certified quality as it is manufactured in a factory and could be applied above untreated work. However, the erection time setting is high, and it is difficult to set in a complex system. A decorative system is more costly and adds an overload to the structure [39, 48]. Boards are shown in Figure 2.3.

(a) **(b)** **(c)**

Figure 2.3 – Fire resistive boards protecting steel structures (a), (b) and (c) (from Ref. [49-51], respectively).

Passive fire protection mortars are one of the most commonly used solutions for their thermal behaviour, which easily complies with the requirements: are less costly than a board protection system, and the application is by spray. So it allows an easy application in complex frames, and surface preparation is not required [18-28]. Aesthetical appearance is the main disadvantage [18], so it is indicated for sheds, industries and non-visible places [39]. It is usually constituted

by cement, gypsum and lightweight aggregates such as perlite and vermiculite. To enhance the mortar's mechanical strength or thermal behaviour, fibres such as polypropylene, glass, steel and hemp are often added [52-54]. Figure 2.4 shows passive fire protection sprayed mortars under and after the application.

(a) **(b)**

Figure 2.4 – Passive fire protection sprayed mortar under application procedure (a) and after the application in steel structures (b) (from Ref. [55-56], respectively).

The EN 1993-1-2 characterizes the unprotected and protected steel temperature development.

2.3 State-of-the-art review

Passive fire protection mortars must have good thermal behaviour to comply with the insulating requirements needed from case to case. Materials commonly used as binders are cement and gypsum due to their vast availability, low cost, ease of production and quality as fire barriers [19, 39, 47, 57-58].

To enhance the material's fire resistance by improving its insulator properties, aggregates are usually introduced into the compositions. The minerals perlite and vermiculite are two of the most commonly used materials [57]. According to Formosa *et al.* [18], PFP mortars with these minerals as lightweight aggregates take benefit of their low thermal conductivity and weight and their capacity to retain water to obtain a porous insulating mortar that is easy to spray.

The main disadvantage of cement based mortars is the pre-existence of micro-cracks which develop into macro-cracks [52]. To restrict the cracks, fibres are added to the composition [59]. However, while the inclusion of metal fibres improves the mechanical strength, polypropylene fibres limit the thermal damage of the mortar [53-54].

Moreover, several studies [60-73] have shown that nanomaterials addition, including nano silica, can improve the mechanical properties of cementitious materials. Despite the knowledge of nano silica in cement based compositions, the addition in gypsum based mortars is still poorly understood. Therefore, it's important to study the materials mentioned above to understand their importance and effect on the composition of passive fire protection mortars.

Perlite is a glassy volcanic rock with large crystals of quartz, alkali feldspar and plagioclase feldspar, formed mainly by SiO_2, with a rhyolitic composition and 2 to 5% of combined water [74]. The combined water is converted to gas at high temperatures and, subsequently, the volume expands 4 to 20 times its original value, forming a lightweight and high porosity material called expanded perlite [75]. Its expanded form has an enhanced capillary action: it is very porous and can hold 3 to 4 times its weight in water [75].

Vermiculite is a hydrated magnesium-aluminium-iron silicate primarily formed by alteration of micaceous minerals due to weathering, hydrothermal action, percolating ground water or a combination of these three factors [74]. Its expanded form is produced by heating the grinded and sieved material to 1000 ºC, converting water into vapour and pushing the layers away from each other in a process called exfoliation [75]. This process modifies the vermiculite structures to granules with accordion shape, lightweight and high porosity [75].

The main advantage of adding these two minerals is the good insulation properties owing to their highly porous nature. However, due to their porous and lightweight nature, their addition drastically modifies the mortar's mechanical characteristics, reducing its compressive and flexural strengths compared to plain cement/gypsum mortars [76]. These statements are confirmed by the literature and this work, as will be seen then.

Gypsum ($CaSO_4.2H_20$) is a mineral used as binder in construction engineering which has a lower calcination temperature than the cement's, within a range of 135 to 180 ºC, reducing CO_2 emissions and becoming an environmentally friendly material [77], furthermore, it has an excellent cost-durability ratio [78-79]. Besides its lightweight and excellent mouldability and sound resistance, it is also a good insulating material as, when subjected to fire, it goes through an endothermic dehydration process which consumes part of fire energy and retards the heat transfer process [79], making its thermal conductivity about six times lower than cement's [73]. However, the main disadvantage of gypsum is its low compressive strength when compared to cement based mortars [79-80] and its poor resistance to water, as prolonged exposure to the atmosphere causes a softening [81]. To solve the second disadvantage, gypsum mortar is recommended in indoor ambient or, if applied on external walls, the process shall include treatment with silicon or bitumen and a plaster coating [78].

Hydrated PC paste consists mainly of calcium silicate hydrate (C-S-H), calcium hydroxide (CH) and calcium sulfoaluminate hydrate ($Ca_6Al_2(SO_4)_3(OH)_{12}\cdot 26H_2O$) [82]. The use of cement based materials for PFP is mostly due to its dehydration process, which occurs gradually and delays the heat transfer. According to Rodrigues *et al.* [59], when cement paste is under high temperatures, the hydrated products gradually lose water, generating water steam and increasing pore pressure within the material. This event starts at 100 °C and continues up to 500 °C, which corresponds to the vaporisation temperature of the crystalline water in the material. At about 300 °C, the interlayer and combined water from C-S-H and sulfoaluminate hydrates would be lost. Further dehydration of the cement paste, due to decomposition of the calcium hydroxide, begins at about 500 °C. Although cement based materials generally provide adequate fire resistance for most applications, their strength and durability properties are significantly affected when subjected to elevated temperatures. For example, in terms of loss in the compressive strength, the critical temperature range is between 600 and 800 ºC [83]. Inclusion of steel fibres could enhance the material thermal and/or mechanical properties, while polypropylene fibres enhance the mortar's thermal behaviour, reducing the cracking process [53]: in the range of 170 ºC, a connecting porosity is created, which contributes to lower vapour pressure and, consequently, reduces cracking process [54].

The addition of nano materials into cementitious compositions is explained by: i) the nanomaterial acts as a void filler due to its nanosized particle also, they cross-linkes in the matrix due to its tubular shape, interacting chemically with Ca^{2+} available in cement paste, thus leads to a denser microstructure and ii) the high amount of silica in the nanomaterial leads to increase the rate of C–S–H due to the consumption of Portlandite in cement matrix [71]. Moreover, using different sizes of nanomaterials may enhance their benefits on the mechanical properties of cement-based mortars even more because it allows a more compact, homogeneous and denser microstructures [73].

Several previous studies are in accordance with the statements mentioned above:

Caetano *et al*. [19] developed and studied a large group of mortars aiming to select the ones with the best thermal behaviour and to compare it with commercial solutions. The specimens were subjected to two types of tests. One of them is an experimental test to analyze the influence of expanded perlite's and expanded vermiculite's grain size on the thermal performance of developed mortars using steel plate moulds exposed to high temperatures on one side up to 900°C. And the second one, an experimental program of tests carried out on twelve steel square section S355 columns protected by the studied mortars under a ISO 834 fire condition and subjected to a preload of 50% of the design value of the load bearing capacity of the columns

at ambient temperature (ULS): 727.8 kN. The bests developed mortar compositions were selected, and their materials were gypsum as binder and expanded perlite or vermiculite as aggregates.

Laím *et al.* [73] concluded that gypsum based mortars have better thermal properties than cement's; however, it has low strength and poor toughness. Moreover, when perlite or vermiculite is added as aggregates, the thermal properties increases, but the mortar's mechanical properties decrease even more.

Mo *et al.* [76] studied the effects of the inclusion of expanded vermiculite in cement based mortar. Three types of composition were produced, one of them constituted by cement and sand and the other two by different amounts of vermiculite added into the cement/sand solution, always with equal water to cement ratios. Following the procedure recommended in EN 12390-5, the compressive test was carried out, and it was observed that the value for the cement/sand mortar had a strength value of 99% higher than the composition with the smallest amount of vermiculite and 173% higher than the composition with the highest amount of the aggregate.

Köksal *et al*. [83] evaluated the combined effect of steel fibres and expanded vermiculite on the properties of lightweight mortar. The compositions had three different amounts of vermiculite, from V/C (vermiculite cement ratio) equal to 4 until V/C equal to 8. The same authors assessed the combined effect of silica fume and expanded vermiculite on the properties of lightweight mortars [84]. They developed twelve compositions, each with different contents of cement to vermiculite. By ultrasonic pulse velocity and flexural and compression tests, it was clear that the samples with smaller quantities of vermiculite presented enhanced strengths and homogeneity.

Köksal's statements [83-84] were also verified by Gencel *et al*. [85]. It was studied the replacement of natural sand with expanded vermiculite in mortars, developing a total of twelve compositions with different contents of binder and expanded vermiculite and submitting the specimens to ultrasonic pulse velocity and compression tests.

Hasanabadi *et al.* [86] assessed the influence of the introduction of expanded perlite and paraffin into cement based compositions. Nine cubic samples were tested under compression at 28 days of age. It was concluded that the addition of lightweight aggregates leads to a decrease of about 60% on the compositions' compression strength.

Ezziane *et al*. [53] evaluated the heat exposure on various types of fibres in mortars' compositions, including polypropylene. The results showed that adding 0.58% of the material

tends to reduce the strength; this effect may be due to poor compaction. At 170 °C, the fibres melted and created the connecting porosity. However, beyond 400 °C, when all the content of the polypropylene fibres has melted, the thermal damage becomes more noticeable. The polypropylene fibres could reduce cracking by controlling the vapour pressures, but it didn't affect the physico-chemical changes. Therefore, this suggests that the tensile strength is more sensitive to cracking than physico-chemical changes, while compressive strength is sensitive to these two phenomena. Including glass and polypropylene fibres into the composition shall enhance thermal and mechanical behaviours. Ezziane *et al*. [54] also assessed the high temperature behaviour of polypropylene fibres reinforced mortars and concluded that introducing these fibres reduces the fracture energy. Also, it was concluded that cement incorporating polypropylene fibre could benefit the mortar and prevent it from spalling because it is melted under a temperature of around 170 °C and, hence, accumulated moisture pressure in mortar can escape through inter-connected pores to the outside of it. Furthermore, at room temperature, the stress transfer between the faces of the cracks by polypropylene fibres was important and gave samples ductility.

Farzadnia *et al.* [71] studied the effect of adding nanomaterials into the compressive resistance of cement based compositions. It was concluded that adding 3% of the material into the composition increased the compressive strength up to 24% compared to the control samples.

Oltulu *et al.* [72] analysed the effect of the addition of nano-SiO_2, nano-Al_2O_3 and nano-Fe_2O_3 powders on cement-based mortars' compressive strengths. After assessing the compressive test results, it was concluded that the addition of nano-SiO_2 increased the compressive strength of mortars.

Laím *et al.* [73] conclude that the addition of nanoparticles to cementitious materials leads to four different types of effects: i) decreases porosity, ii) increases durability, iii) behaves as an activator that promotes pozzolanic reactions and iv) enhances the microstructure of the cement by consuming portlandite crystals by decreasing their orientation, reducing their size. After an extensive review, it was also concluded that adding nano silica particles led to an improvement in the compressive strength of the mortar of 54%, compared to mortars without this material, at 28 days of age.

2.4 Challenges

As mentioned before, the present work is within the scope of Nanofire project and it is composed by several other investigations. The first challenge was to study the bests materials

to include into the developed mortars' compositions. Then, dozens of mortars were developed and were set to experimental tests to determine the top thermal performances.

With the collected data, two gaps were created: thermal and mechanical characterisation needed to be performed. As mentioned, the inclusion of light weight materials, such as EP and EV, increases the thermal and decreases the mechanical performances. Passive fire protection mortars mostly have to attend thermal requirements, however, beside formal and commercial requirements, its mechanical characterisation is important to guarantee the flexibility of the materials to accommodate the structure's displacements.

Thus, two works were performed to fill up the thermal and the mechanical characterisation gaps. The present work attend the mechanical characterisation gap and is correlated with the thermal characterisation work as it is expected that the mortars with the best thermal performance has the lowests mechanical strengths, according to the literature.

3 MATERIALS AND METHODS

3.1 Materials and compositions

Based on a previous experimental campaign [19], it was possible to identify three laboratory developed mortars with the best thermal performances (CV, GP and GV) and the best commercial passive fire protection solution used as reference composition (C). With the addition of nano and micro silica, three other compositions were made from laboratory developed mortars: CV.NMS, GP.NMS and GV.NMS. The following materials were used in the compositions of the mortars: commercial passive protection solution (CPPS), Portland cement CEM II/B-L 32.5 (PC), the gypsum powder (GY), expanded perlite (EP), expanded vermiculite (EV), polypropylene fibres with an average diameter of 31 μm and an average length of 6 mm (PP), silica microparticles with an average diameter of 1000 nm (MS), silica nanoparticles with an average diameter of 200 nm (NS) and water (W). The granulometry of CPPS, PC, GY, EP and EV is shown in Table 3.1. The EP and EV grains were submitted to the milling procedure, according to [19].

Table 3.1 – Granulometry of the materials used in the mortars' compositions.

	Particle Size (mm)									
Material	**> 1.400 (%)**	**1.400 (%)**	**1.000 (%)**	**0.500 (%)**	**0.355 (%)**	**0.250 (%)**	**0.180 (%)**	**0.125 (%)**	**0.090 (%)**	**0.025 (%)**
CPPS	0.21	1.44	7.90	5.56	16.69	5.46	7.29	14.39	40.84	0.21
PC	0.00	0.00	0.19	0.16	3.22	1.53	0.72	8.32	72.43	13.43
GY	0.22	2.72	11.52	7.84	28.54	9.52	4.79	13.30	21.54	0.01
EP	0.21	0.60	6.39	5.06	12.78	3.94	2.60	19.13	49.27	0.00
EV	2.69	25.02	32.15	9.94	11.86	4.86	4.50	3.36	5.61	0.01

The mortars are referenced as C, CV, CV.NMS, GP, GP.NMS, GV and GV.NMS, where C stands for the commercial solution, CV for cement-vermiculite, CV.NMS for cement-vermiculite with nano and micro silica (NMS) particles, GP for gypsum-perlite, GP.NMS for gypsum-perlite with NMS particles, GV for gypsum-vermiculite and GV.NMS for gypsum-vermiculite with NMS particles. Compositions of the mortars are presented in Table 3.2.

Table 3.2 – Composition of the selected mortars – amount of materials (%) in volume (adapted from [19]).

Mortar Designation	**CPPS**	**PC**	**GY**	**EV**	**EP**	**PP**	**NMS**	**W/B**
C	100%	-	-	-	-	-	-	0.60*

CV	-	49%	-	50%	-	1%	-	2.00
CV.NMS	-	48%	-	50%	-	1%	1%	2.40
GP	-	-	40%	-	60%	-	-	1.08
GP.NMS	-	-	39%	-	60%	-	1%	1.04
GV	-	-	75%	25%	-	-	-	0.70
GV.NMS	-	-	74%	25%	-	-	1%	0.66

* Water commercial solution ratio in weight %.

Cement and gypsum based mortars demand a certain amount of water for their manufacture. However, the water to binder ratio is between 1/3 and 1/5.3 [87] for cement and gypsum based mortars, respectively. It's possible to see the higher water to binder ratios among the developed mortars due to the addition of hygroscopic materials such as EP and EV [87]. As higher is the content of EP and EV, higher is the W/B, for the different types of binders.

CIMPOR produced the PC, and the GY was supplied from PTFLIX SUPER PLUS, both from Portugal, the EP and EV from PROJAR, Spain, the PP from DURO FIBRIL, Portugal, and the NMS were manufactured at the Department of Chemical Engineering of the University of Coimbra and its manufacturing was in accordance with the exposed by Vaz-Ramos *et al.* [88]. The raw materials are shown in Figure 3.1.

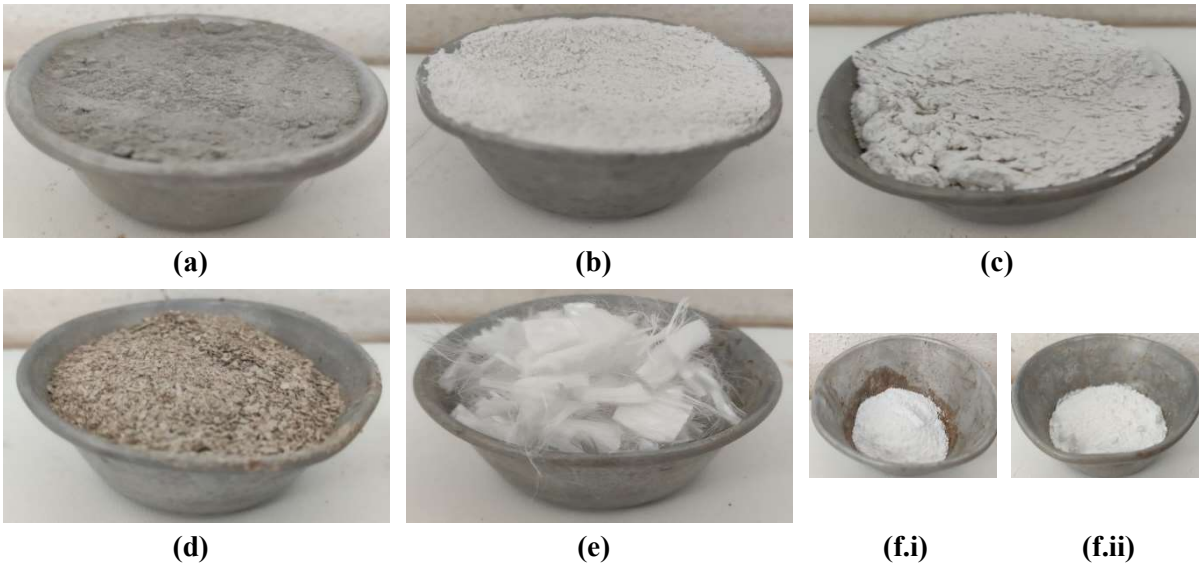

Figure 3.1 – Raw materials utilized in the manufacturing of the mortars: PC (a), GY (b), EP (c), EV (d), PP (e), NS (f.i) and MS (f.ii).

3.2 Experimental program

Mixtures were prepared at the Department of Civil Engineering of Coimbra University, Portugal, while tests were conducted at the Department of Mechanical Engineering. The experimental program included four different tests, among non-destructive and destructive tests, to characterize the mortars' mechanical properties: i) an ultrasonic pulse velocity (UPV) test and ii) an impulse excitation of vibration (IEV) test, as the non-destructive tests, and iii) a flexural (FL) and iv) a compression (CP) tests, as the destructive tests. The experimental program of tests is summarized in Table 3.3.

The non-destructive program characterised the mortars' Young's modulus, the shear modulus and the Poisson's ratio through UPV and IEV tests. Two types of specimens followed each standard recommendation: a 160 x 40 x 40 mm specimen was used in UVP tests and a 200 x 100 x 20 mm specimen in IEV tests.

The destructive tests defined the mortars' flexural and compression strengths. Following the respective standards recommendations, the 160 x 40 x 40 mm specimen was subjected to the flexural test. After its collapse, it was divided into two 80 x 40 x 40 mm halves and subjected to the compression test.

Table 3.3 – Experimental program tests of the different specimens.

Mortar Designation	**160 x 40 x 40 mm specimen**		**80 x 40 x 40 mm specimen**	**200 x 100 x 20 mm specimen**
	UPV test	**FL test**	**CP test**	**IEV test**
C	4	4	6*	1
CV	4	4	8	1
CV.NMS	4	4	8	1
GP	4	4	8	1
GP.NMS	4	4	8	1
GV	4	4	8	1
GV.NMS	4	4	8	1

* Two specimens had no data collected.

To obtain a better correlation, only three specimens' results with the lower standard deviation were selected for each mortar and test type. The results were collected according to the respective regulation, the average values were defined, and the compositions' final results were characterized.

3.3 Preparation of the specimens

For the fabrication of the mortars, a 0.01 grams precision balance, a Hobert N50 mixer with 5 litres of capacity (Figure 3.2a), a graduate beaker and a stainless-steel lab spatula (Figure 3.2b) were used. The procedure followed the steps: 1) The raw materials were weighed and placed inside the mixer container; 2) the mixer was put into operation for 5 minutes at a slow speed and, at the same time, the corresponding amount of water was added; 3) the mortar was manually kneaded with a spatula to remove parts of the mortar that were on the walls of the container and thus homogenize the mixture, then returning the container to the mixer; 4) for the mortars with NMS particles and aiming its activation, 2.4 grams of NMS particles were placed in a 45 millilitres water solution and submitted to ultrasounds for twelve hours, using Retsh equipment (Figure 3.2c); and 5) the mortar was placed inside the mould.

(a) **(b)** **(c)**

Figure 3.2 – Equipment used for the fabrication of the mortars: Hobert N50 mixer with 5 litres of capacity (a), graduate beaker and stainless-steel lab spatula (b) and Retsh ultrasounds equipment (c).

A total of 7 and 42 specimens were cast in 200 x 100 x 20 mm and 160 x 40 x 40 mm steel moulds, respectively. The mixtures were placed inside the mould, compacted by manual vibration, and the upper faces were cleaned up and flattened. Forty-eight hours after casting, the specimens were demoulded and submitted to 28 days curing process in the laboratory environment with a controlled temperature (25 °C) and relative humidity (RH) of 55%. To minimize possible effects that temperature and humidity might have on the properties of each mortar composition, all composition mixtures were manufactured on the same day. The specimens were submitted to the experimental tests after six months of age.

The specimens inside the moulds and their schematic representation are shown in Figure 3.3.

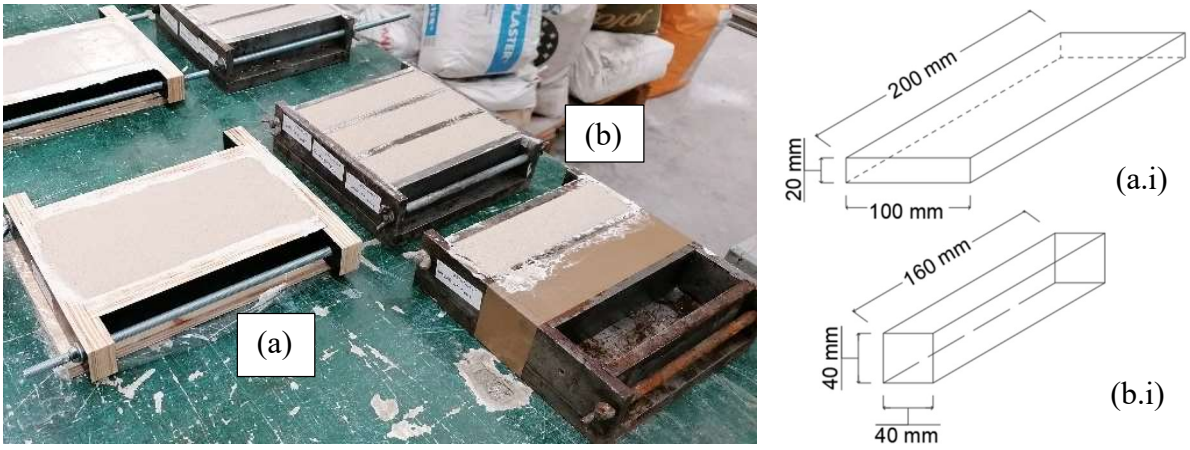

Figure 3.3 – 200 x 100 x 20 mm and 160 x 40 x 40 mm specimens inside the moulds (a) and (b) and their schematic representation (a.i) and (b.i), respectively.

For SEM analysis, it was taken care to polish the samples with fine paper to avoid filling the pores with particles. To obtain clear images and proceed to the analysis, the samples were coated with a 4 nm layer of gold, as the granules are nonconductive in vacuum (Figure 3.4).

(a) **(b)** **(c)**

Figure 3.4 – Samples before (a), during (b) and after (c) the gold coating process.

3.4 Experimental testing system and procedure

3.4.1 Non-destructive tests

The UPV tests collected the propagation velocities of the compression and shear waves by inducing the specimen to repetitious pulses by a pulse generator. The tests were carried out under the ASTM D 2845-05 [89] recommendations, and Pundit Lab equipment was used.

The IEV tests were carried out using PICO equipment under ASTM E 1876-01 [90] standard recommendations. The experimental test consisted in inducing a manual excitation by a singular strike by an impulser (in this case, a steel sphere fixed to the end of a flexible polymer rod) to obtain the specimens' mechanical resonant frequencies.

Both tests had the same objective: to determine the specimens' dynamic properties. The properties were calculated through normalized equations, defined in both standards. The elastic constants determined by the UPV test method are termed ultrasonic since the pulse frequencies used are above the audible range so they may differ from those determined by other dynamic methods. Hence, the two different dynamic tests were carried out.

3.4.1.1 Ultrasonic pulse velocity test

Under the before mentioned standard recommendations, the experimental testing system setup is represented in Figure 3.5.

It consisted of a 160 x 40 x 40 mm specimen (a); a pulse generator (b) which applies pulses with variable width repeatedly on the specimen; two types of transducer: a 54 kHz capacity (c) for the determination of P waves (longitudinal or primary waves, V_p) and a 1 MHz capacity (d) which determines the S waves (shear or secondary waves, V_s), both consists of a transmitter that converts electrical pulses into mechanical pulses and a receiver that converts mechanical pulses into electrical pulses; a computer (e) that contains the equipment's software which displays the on-time readings, the graph and its parameters; and a support (f) to accommodate the specimen in the correct position.

It is important to refer that the energy transmission between the transducer element and test specimen was improved by lapping the surfaces of the face plates to make them smooth, flat, and parallel and by coupling the transducer element to the face plate by a thin layer of Vaseline gel, an electrically conductive adhesive.

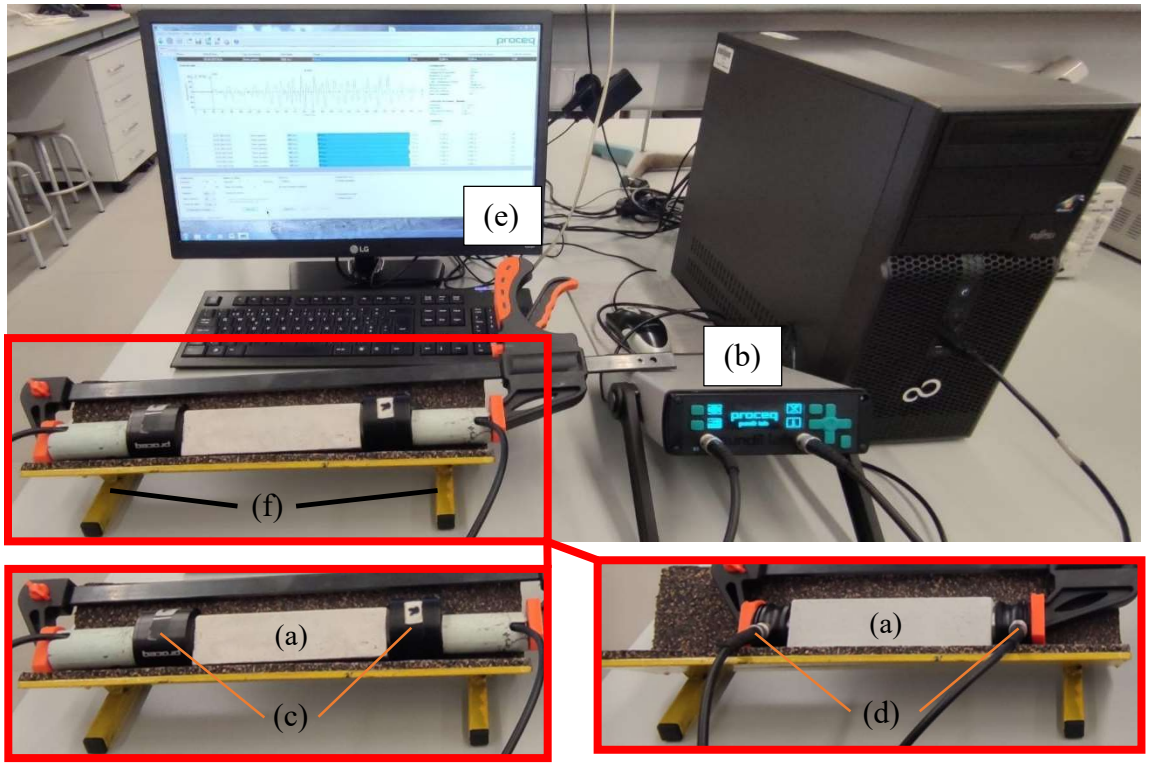

Figure 3.5 – UPV test setup: specimen (a), pulse generator and display unit (b), longitudinal waves transducer (c), shear waves transducer (d), computer (e) and support system (f).

Before proceeding to the readings, a pulse length was set, probe a frequency and pulse amplitude (Table 3.4) by a trial-and-error process, following the equipment's recommendations.

Table 3.4 – Parameters values for compression and shear waves procedure.

Wave Type	Pulse Length	Probe Frequency	Pulse Amplitude
Longitudinal	9.3 µs	54 kHz	125 V
Shear	2.0 µs	250 kHz	500 V

3.4.1.2 Impulse excitation of vibration test

The IEV test method is specifically appropriate for determining elastic, homogeneous, and isotropic materials' modulus. The specimen's dimensions differ from the others tests due to its standards recommendation, which indicates a ratio width to thickness of five or greater. This ratio minimizes experimental difficulties during the shear modulus measurement.

The experimental testing system (Figure 3.6) consisted of a 200 x 100 x 20 mm mortar specimen (a); a impulser (b); a 10 kHz frequency capacity transducer (c) in direct contact with the specimen to detect and transport the frequencies waves; an electronic system (d) to amplify, to read and to analyze the signals received; a computer (e) to display the waves that determine the frequencies and two types of supports: support for the longitudinal frequency measurement (f.i) and the torsional frequency measurement (f.ii). The first support system consisted of two supports spaced by 0.224 L (L being the specimen's length) from the borders, and the second support system consisted of cross-shaped support located at the midpoint of the specimen's length and width.

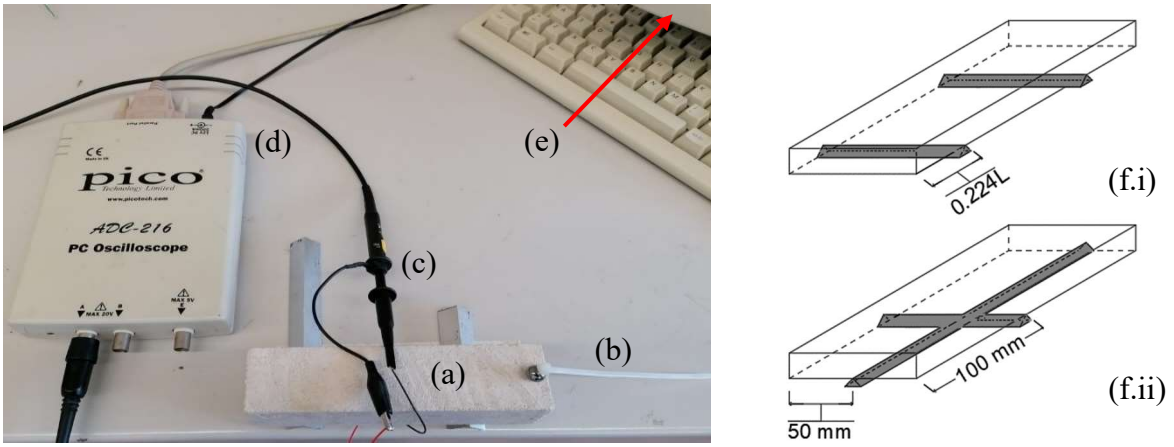

Figure 3.6 – IEV test experimental setup representation: test specimen (a), impulser (b), transducer (c), electronic system (d), computer (e), schematic representation of the longitudinal (f.i) and the transversal (f.ii) frequencies measurement.

In an illustrative way, Figure 3.6 contains a 160 x 40 x 40 mm specimen instead of a 200 x 100 x 20 mm. This is explained due to the usage of the wrong type of specimen at the beginning of the experimental programs. After verifying that the dimensions had to have a ratio width to thickness of five or greater, specimens 200 x 100 x 20 mm were used, however, no photo was taken.

The transducer location was set in the proper location to measure the desired vibrations mode, following the standard recommendation. It was taken special care that the transducer's location remains similar within multiple readings, as well as the force used on the impulser.

3.4.2 Destructive tests

The destructive tests took place in a SHIMADZU compression-tensile machine. The flexural test followed the European standard EN 12390-5 [91] and the compression test, EN 1015-11 [92].

It is important to mention that, in the flexural test, the specimens were subject to a bending moment by applying load through two upper and two lower rollers while, in the compression test, through a 40 x 40 mm steel plate. The objective of selecting a four-point flexural test was to reduce to zero the shear strength at midspan, thus, producing a pure bending moment at that point.

A constant displacement of 0.005 mm/s was applied to the specimen, and the computer registered the force (N) needed to generate this displacement. The test ended when no greater load could be sustained (collapse). The maximum loads recorded are the outputs needed to determine the flexural and compression strengths, following the respective standards normalized equations.

It is important to highlight that the standard velocity is 0.001 mm/s. However, a velocity of 0.005 mm/s was adopted because preliminary tests showed that no deviation of results has occurred even with a velocity five times faster.

The experimental testing system (Figure 3.7) consisted of a compression-tensile machine of 100 kN capacity (a); two types of support system (b.i and b.ii) for each test; a load cell (c); a computer (d) equipped with the machine's software for data acquisition; and by a 160 x 40 x 40 mm (e.i) and a 80 x 40 x 40 mm (e.ii) test specimens in the flexural and compression tests, respectively. Also, a schematic representation of both support systems (f.i and f.ii) is shown for better visualisation.

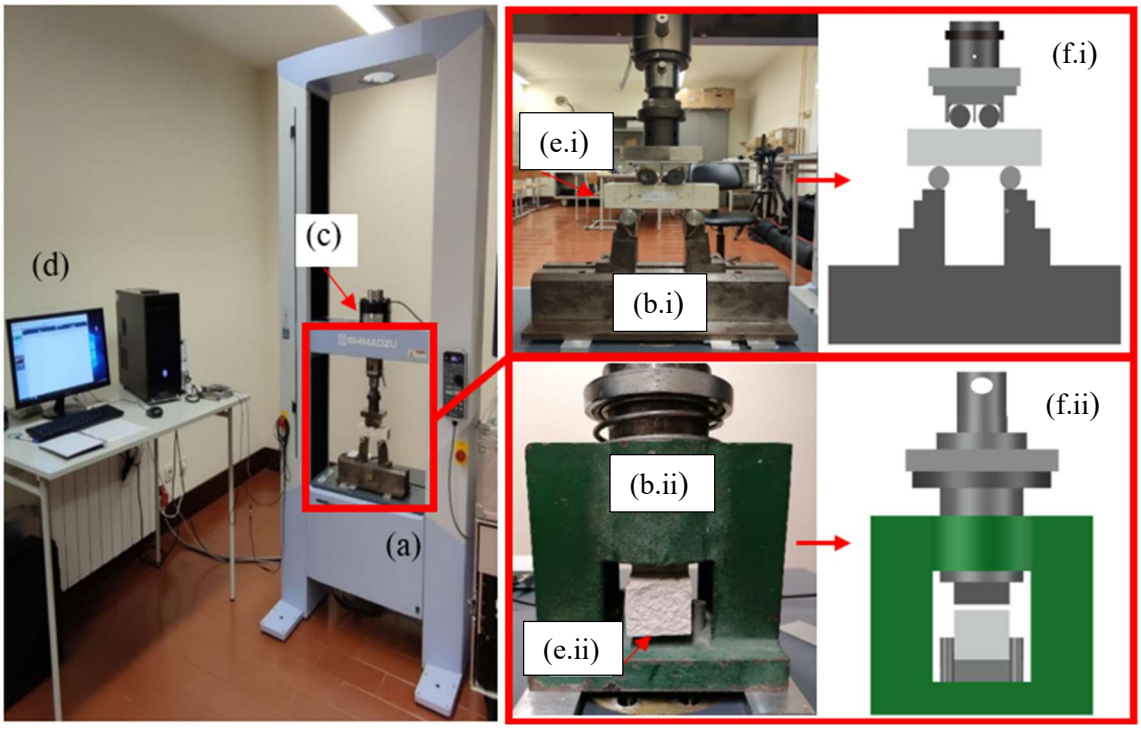

Figure 3.7 – Experimental test setup representation for both destructive tests: test machine SHIMADZU (a), flexural (b.i) and compression (b.ii) support systems, load cell (c), computer (d), flexural (e.i) and compression (e.ii) tests specimens and flexural (f.i) and compression (f.ii) support systems schematic representation.

3.4.2.1 Flexural test

The support system consisted of two supporting rollers (on the bottom) and two upper rollers, which equally divided the load the machine applied. Three rollers, including the two upper ones, could rotate freely around their axis and be inclined in a plane normal to the longitudinal axis of the test specimen. These support conditions reduce friction forces between the rollers and the specimen.

The supporting rollers have a circular cross-section with a diameter of 25 mm. The specimens' surfaces were cleaned up, aiming to eliminate other particles to avoid additional friction resistance. Before and during the procedure, all vertical planes of the supports were parallels, while the specimen's and the load cell's geometric centres were aligned.

3.4.2.2 Compression test

The support system was defined by a hollow steel rectangular box (160 x 120 x 215 mm) opened on two parallel sides and equipped with a 40 mm square section piston on the top, pushed by the load cell that transfers the load as a pressure to the specimen.

The tests were carried out on each half of the specimens after the breakage after the flexural test. All surfaces were cleaned up to avoid additional friction resistance, the specimen's and piston's geometric centres were aligned, and the load was applied to the specimen's face cast against the face of the mould.

4 RESULTS AND DISCUSSION OF THE MECHANICAL AND THE COMPLEMENTARY TESTS

4.1 Complementary tests

The non-destructive's test results are highly dependent of the specimens' physical parameters, such as mass and dimensions. Furthermore, it is well known that insulating materials have decreased mechanical strengths due to their porous structure. However, present a lower mechanical loss under high temperatures [93-100]. Given the importance, density and porosity were determined according to ASTM C20-00 [101] and to ISO/DIS 15901-1 [102] standards recommendations, respectively. Furthermore, the mass loss as a function of temperature was determined by a TGA analysis, the identification of crystalline phases of materials by XRD and the image microstructure by SEM.

The density (ρ) evaluation used a 0.01g precision scale and a 0.01mm precision electronic pachymeter (Figure 4.1). The porosity evaluation was carried out at IPN using a Mercury porosimetry procedure, which measures inter-particle and intra-particle porosity. Both tests were carried out at room temperature (25 ºC).

(a) **(b)**

Figure 4.1 – 0.01g precision scale (a) and a 0.01mm precision electronic pachymeter (b).

In Figure 4.2, it is possible to see the density and porosity tests results:

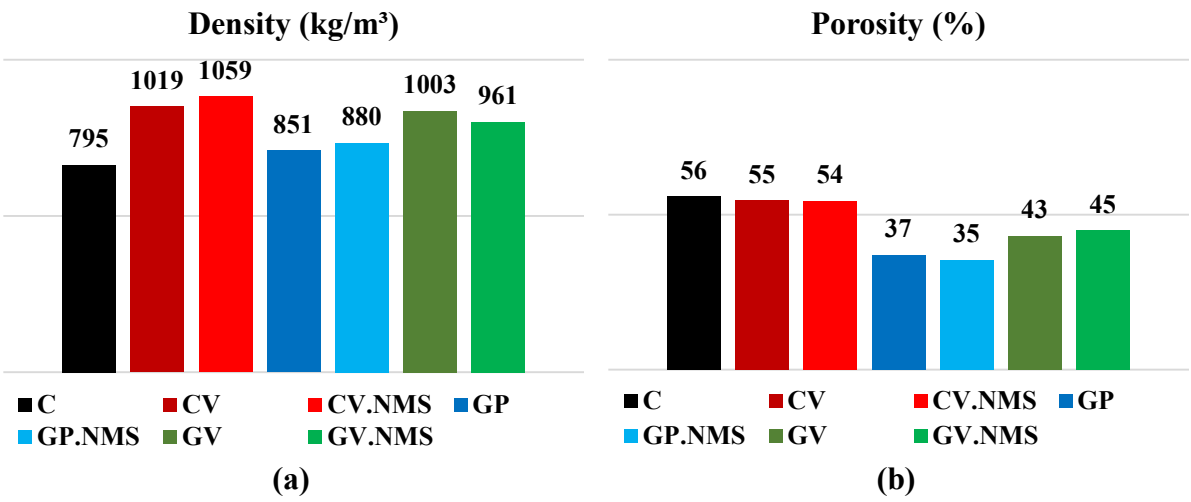

Figure 4.2 – Mortars' average density (a) and porosity (b).

A notorious variation between the densities was measured. The commercial solution has the lowest density, about 22%, 25%, 7%, 10%, 21% and 17% lower than CV, CV.NMS, GP, GP.NMS, GV and GV.NMS, respectively. The differences in densities between the gypsum based mortars are due to two factors: i) the higher apparent density of EV when in comparison to the EP's as they have maximum values of 192 kg/m^3 [103] and 100 kg/m^3 [104], respectively, and ii) the different amount of binder into the compositions. Among the cement based and gypsum based mortars, the variation in densities is due to the difference in the specific weight of cement (1900 to 2300 kg/m^3) and gypsum (1200 to 1800 kg/m^3), according to EN 1991-1-1 [105].

Concerning the porosity rates, the mortars C, CV and CV.NMS stands out as the ones having the highest porosities. The commercial solution has the highest rate, about 2%, 4%, 51%, 60%, 30% and 24% higher than CV, CV.NMS, GP, GP.NMS, GV and GV.NMS, respectively. The elevated porosity percentage of CV and CV.NMS is due to the high amount of water used to fabricate the mortars. The cement uses the water for its hydration, however, the remaining water stays cloistered inside the mortar, and, after the six months of age, this water evaporates, forming voids. The sizes of EP and EV's particles led to a notorious difference between the gypsum based mortars' porosities. As shown in Table 3.1, about 50% of EP particles have a size of 0.090 mm, while about 65% of EV's have a size between 1.400 and 1.000 mm. This led to GP and GP.NMS group to present the lowest values of porosity.

It can be observed that the NMS addition didn't show considerable effects on both parameters as CV.NMS/CV, GP.NMS/GP and GV.NMS/GV densities ratios are 1.04, 1.03 and 0.96, respectively, and porosities ratios are 0.98, 0.95 and 1.05.

The weight loss with increasing temperature of the compositions was analyzed by TGA (Figure 4.3). It was tested the commercial solution and GP.NMS (the composition which had the best thermal behaviour) [19]. The test consisted in powder samples heated from room temperature to 1000 °C, at a heating rate of 10 ºC/min, in air atmosphere. The tests were carried out in NETZSCH TG 209F1 Libra equipment.

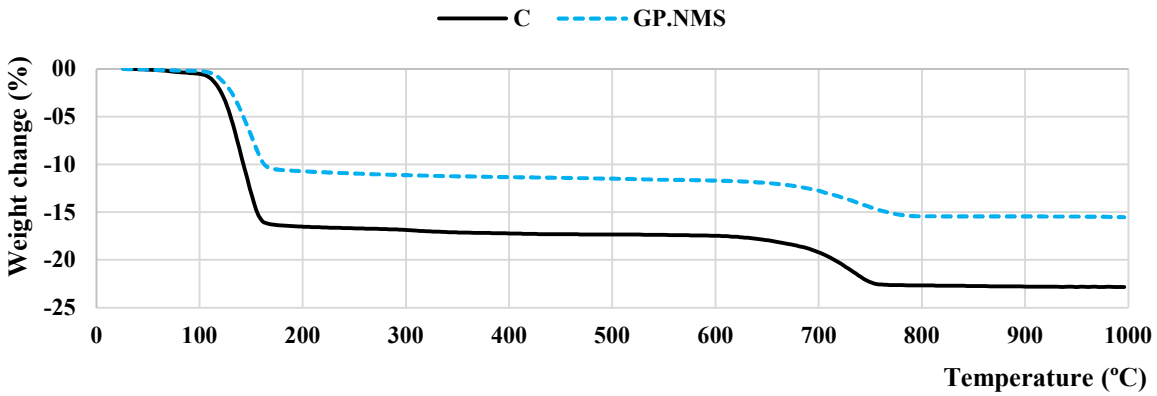

Figure 4.3 – C and GP.NMS compositions' TGA data.

To allow further insight into the mineralogy of the GY, EP, EV and NMS, the XRD test was carried out, and the results are presented in Figures 4.4 and 4.5 for C and GP.NMS composition, respectively. The tests were carried out in a Philips X'Pert – MPD diffraction with cobalt (kα1= 1.78897 Å) radiation, with steps of 0.025º and 2 seconds per step, between 4 and 100°, two theta.

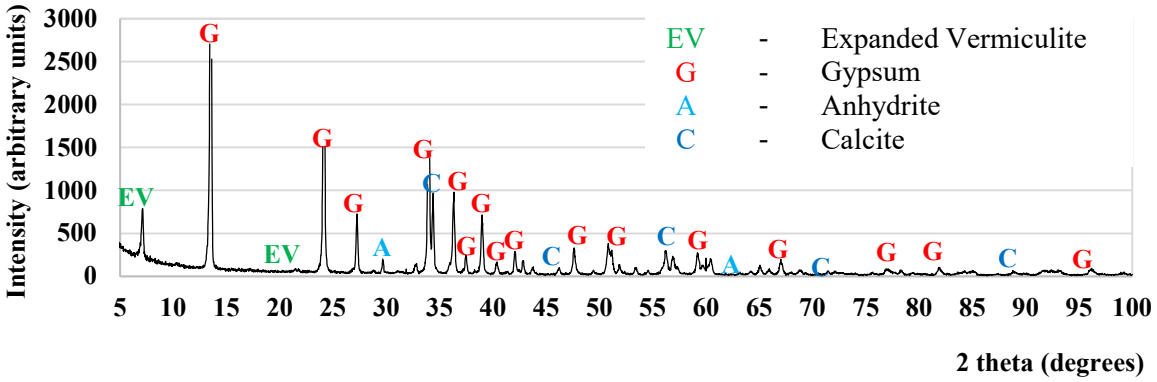

Figure 4.4 – C composition's XRD data.

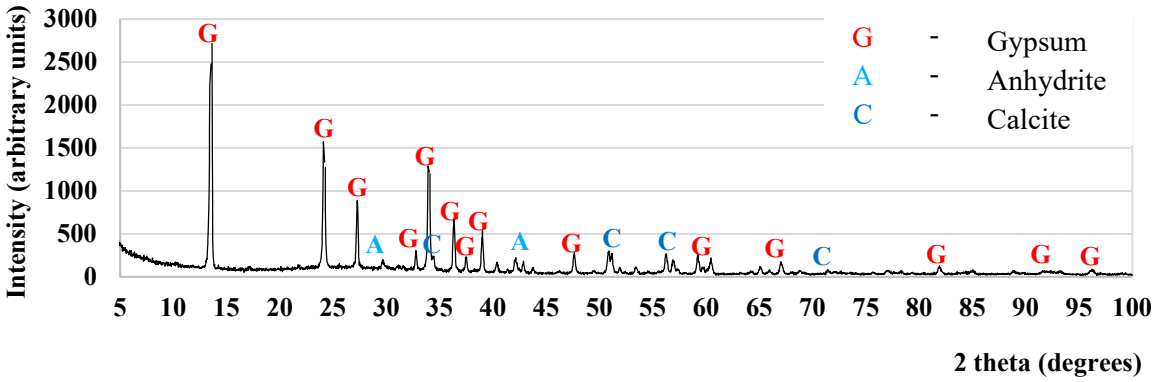

Figure 4.5 – GP.NMS composition's XRD data.

By the assessment of the TGA results, it is clear that the first peak of weight loss occurred between 100 and 170 ºC, and the second was between 600 and 790 ºC. Both curves are similar in their behaviour, only having a notorious difference concerning the weight loss: GP.NMS lost 10.4% and 15.5% of its initial weight at 170 and 1000 ºC, respectively, while C, 15.9% and 22.8% at 170 and 1000 ºC, respectively.

In general, dehydration of gypsum takes place at a temperature range between 80 and 250 ºC, depending on the gypsum's heating rate and composition. In this case, nearby 100 ºC, the first dehydration occurs ($CaSO_4 \cdot 2H_2O \rightarrow CaSO_4 \cdot 0.5H_2O$), and nearby 130 ºC, the complete dehydration takes place ($CaSO_4 \cdot 0.5H_2O \rightarrow CaSO_4$). The typical behaviour between the compositions is in accordance with the gypsum TGA behaviour [47, 81, 105-106]. However, there are two cases of the development of the second peak: 1) According to Wakili *et al.* [47], the second peak occurs due to the decomposition of calcium carbonate, present in the industrial gypsum chemical structure, turning into calcium oxide and carbon dioxide and, according to Azdarpour *et al.* [106], the second peak occurs due to evaporation of sulphate phases as the reaction SO_4 to SO_3 occurs above 550 ºC and SO_3 to SO_2, above 700 ºC.

By assessing XRD and TGA results, it's determined that the commercial solution is formed mainly by gypsum, about 70%, with the remaining 30% being EP, EV and other unknown materials. The XRD results show that both compositions (C and GP.NMS) present similar gypsum's crystalline phases [80, 105-107]. Furthermore, GP.NMS' results indicate the existence of an amorphous between 15 and 45º, two theta, which is a characteristic of EP [108-109]. Adding perlite and vermiculite in their expanded forms decreases the weight loss of gypsum based mortar due to their insulating properties, as previously mentioned [87, 106, 109-111]. However, this situation could only be seen in GP.NMS as the weight loss of C is similar to the pure gypsum's weight loss, according to the literature.

In conclusion, in both cases, the formation of the first peak is due to the gypsum's dehydration, and of the second peak, the decomposition of calcium carbonate and the evaporation of sulphate phases. Furthermore, the difference in weight loss is due to the percentage of the content of insulating aggregates, EP and/or EV, in the composition.

The morphology and microstructures of the mortars were observed through HITACHI SU3800 SEM equipment. SEM images are shown in Figure 4.6.

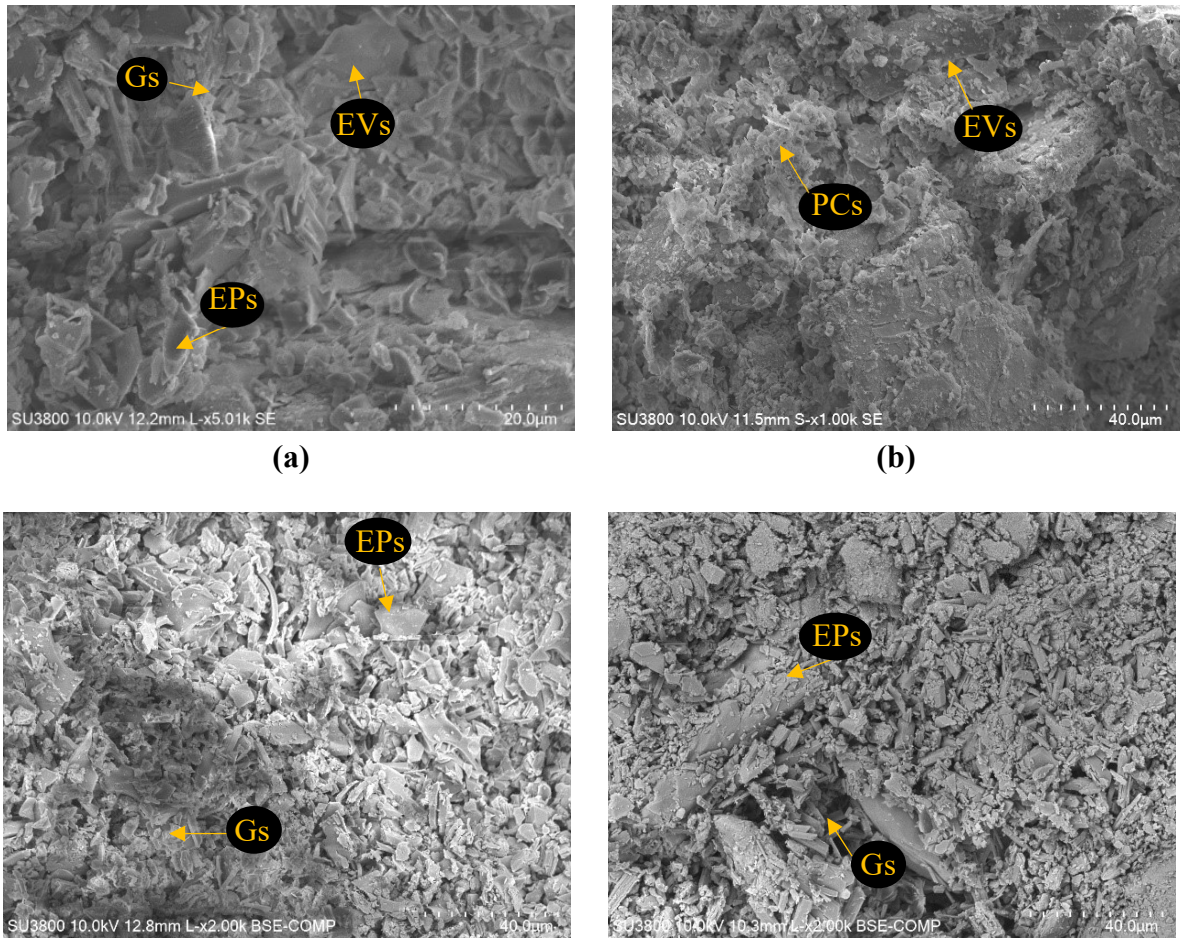

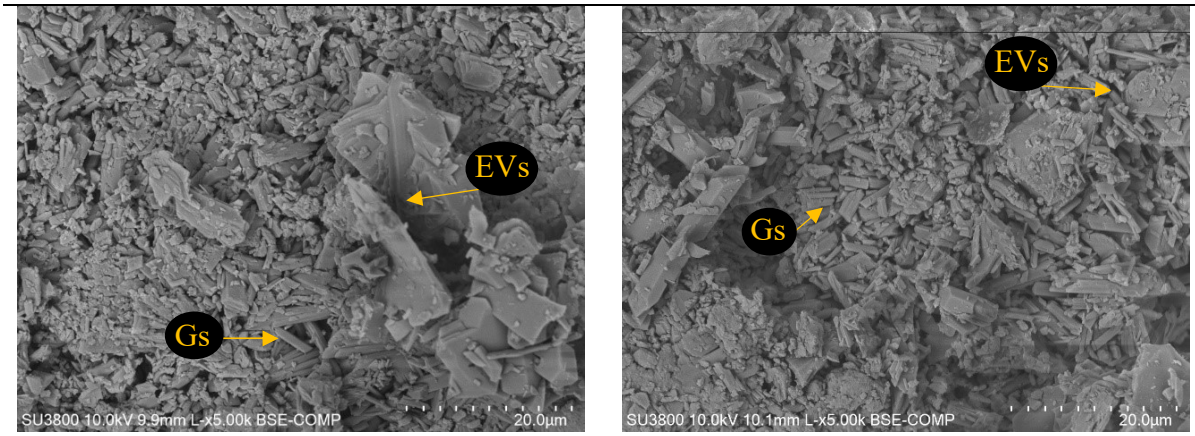

(e) **(f)**

* CV image isn't available due to a malfunction of the machine.

Figure 4.6 – SEM images of the various compositions: C, CV.NMS, GP, GP.NMS, GV and GV.NMS represented in (a), (b), (c), (d), (e) and (f), respectively. Gp stands for Gypsum structure, Eps for expanded perlite's, EVs for expanded vermiculite`s and PC's for cement`s.

SEM analysis shows a common type of structure between the compositions due to the similarity of materials used and also differences in porosity of the compositions because of C and CV.NMS presents a higher percentage of voids. The gypsum is mainly formed by prismatic shape crystal structures, with an average length of 4 µm to 6 µm, in accordance with the literature [81, 105, 111-113]. EP and EV show a lamellar shape with different lengths but always longer than the gypsum structures. The formation and distribution of the structures are in accordance with several previous studies [86, 104, 111-114]. The PC random and isotropic structure satisfys the structures from the literature [115-117], also no degradation of portlandite and C-S-H is seen. According to Rodrigues *et al.* [59], the degradation of these solids starts above 550 ºC.

Due to the reduced quantity of PP and NMS, it wasn't possible to visualize them in the presented SEM analysis images. The PP has only been seen with a zoom 60% lower than the used. According to Wang *et al.* [117] and Lim *et al.* [118], an approach using EDS spot analysis and BSE micrographs would be possible to identify the NMS.

4.2 Non-destructive tests

4.2.1 Ultrasonic pulse velocity test

After the experimental procedure, it was possible to obtain the propagation velocities of longitudinal and shear waves (V_p and V_s, respectively) and, using the following equations, to determine the Young's modulus (E), the shear modulus (G) and the Poisson's ratio (μ):

$$E = [\rho V_s^2 (3 V_p^2 - 4 V_s^2)]/(V_p^2 - V_s^2) \quad \text{(Eq. 1)}$$

$$G = \rho V_s^2 \quad \text{(Eq. 2)}$$

$$\mu = (V_p^2 - 2 Vs^2)/[2(V_p^2 - Vs^2)] \quad \text{(Eq. 3)}$$

The specimens' mechanical properties obtained by the UPV tests are shown in Table 4.1.

Table 4.1 – Ultrasonic pulse velocity test results.

Designação da Argamassa	V_p (m/s)	V_s (m/s)	E (GPa)	G (GPa)	μ
C	1899	1192	2.656	1.130	0.18
CV	1033	537	0.772	0.294	0.32
CV.NMS	1147	575	0.933	0.350	0.33
GP	1289	751	1.192	0.488	0.23
GP.NMS	1284	756	1.212	0.491	0.23
GV	1831	1105	2.913	1.217	0.21
GV.NMS	1743	1069	2.674	1.116	0.20

4.2.2 Impulse excitation of vibration test

After the experimental procedure and the frequencies readings, it was determined the Young's modulus by the following equation:

$$E = 0.9465 (m f_f^2 / b)(L^3 / t^3)T_1 \quad \text{(Eq. 4)}$$

where m stands for the mass of the bar (g), b for the width of the bar (mm), L for the length of the bar (mm), t for the thickness of the bar (mm), f_f for the fundamental resonant frequency of bar in flexure (Hz) and T_1 for the correction factor for the fundamental flexural mode to account for finite thickness of bar and Poisson's ratio.

The dynamic shear modulus was obtained through the following equation:

$$G = 4 L m ft^2 [B / (1 + A)] / b t \quad \text{(Eq. 5)}$$

where f_t stands for the fundamental resonant frequency of bar in torsion (Hz), B and A are only dependent of the specimen's dimensions.

Finally, the Poisson's ratio is given by the Equation 6:

$$E/G = 2(1+\mu) \quad \text{(Eq. 6)}$$

The IEV tests results are shown in Table 4.2.

Table 4.2 – Impulse excitation of vibration test results

Designação da Argamassa	f_f (Hz)	f_t (Hz)	E (GPa)	G (GPa)	μ
C	972	1114	2.601	1.091	0.19
CV	464	506	0.753	0.283	0.33
CV.NMS	536	582	0.910	0.344	0.32
GP	667	756	1.381	0.564	0.22
GP.NMS	666	755	1.293	0.533	0.21
GV	950	1077	2.721	1.111	0.22
GV.NMS	867	999	2.708	1.118	0.20

4.2.3 Discussion of the tests results

Through the assessment of non-destructive test results, the mechanical properties of the developed mortars were compared. Also, it allows evaluating the influence of the binder and aggregates and the addition of nano and micro silica particles.

Studies highlights that as higher is the non-destructive tests' values of velocities/frequencies, the greater is the quality of the mortar's uniformity and homogeneity [83-85]:

Köksal *et al*. [83] evaluated the effect of expanded vermiculite on properties of lightweight mortar. It was produced three different compositions, and it was expected that the ones with a higher amount of aggregate lead to lower velocities due to the high amount of air inside the voids, and the results confirmed it: the composition with the lower content of vermiculite had a velocity around 11% and 21% higher than the other two, respectively. The same author also assessed the effect of expanded vermiculite and other materials on the properties of three other lightweight mortars [84]. The higher the vermiculite to binder ratio (V/B), the lower the velocities. The composition with the highest binder content had an average velocity (2367 m/s) of 5% and 11% higher than the other, respectively.

Gencel *et al.* [85] studied the replacement of natural sand with expanded vermiculite: the compositions without vermiculite added had an ultrasonic pulse velocity of 2800 m/s, the 15% vermiculite by weight composition had a velocity of 2660 m/s and the 30% vermiculite by weight composition, 2330 m/s.

Figure 4.7 presents the correlation between the velocities and frequencies and the binder content for each composition.

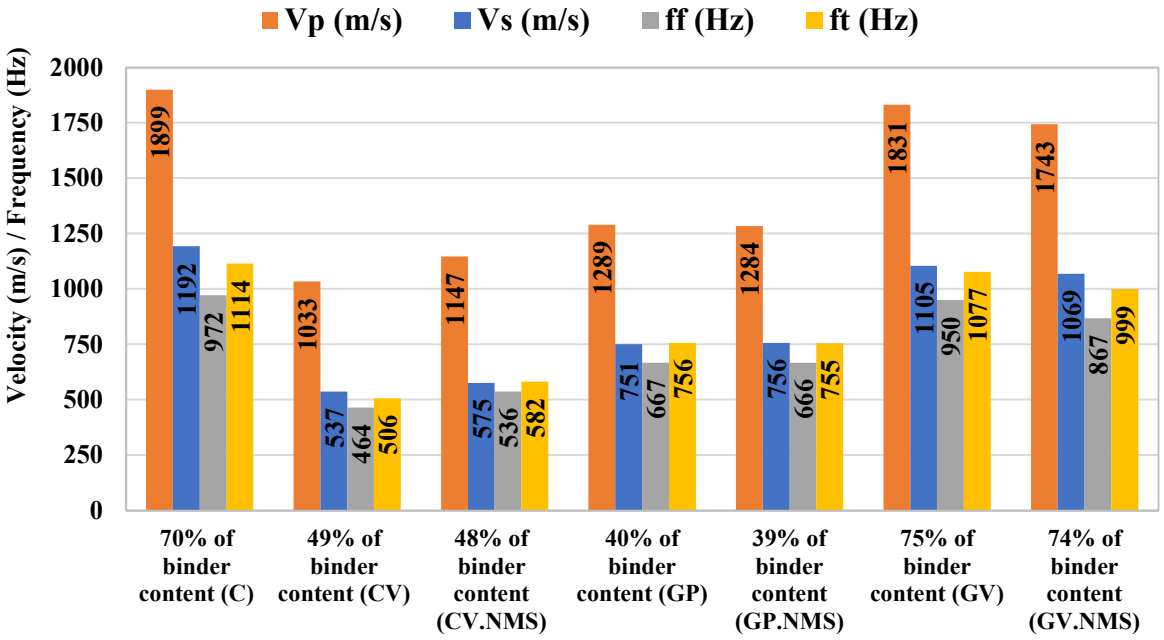

Figure 4.7 – UPV velocities (m/s) and IEV (Hz) frequencies in the function of the binder content.

As shown in Figure 4.7, and according to the literature review, the results obtained from the non-destructive tests show that the velocities/frequencies increase as the binder content increases. Analyzing the results of the gypsum based mortars developed in the laboratory, GV has the highest amount of binder and it can be seen that it has the highest values of velocities and frequencies, while P.NMS has the lowest values. Comparing the values of velocities and frequencies between EP and EV when increasing 1% of binder into the composition, GV showed a 6.4% average increase in its properties compared with GV.NMS; however, GP and GP.NMS didn't show considerable differences. Moreover, these results show that, for the tested dosages, the addition of nano and micro silica particles slightly influences the alteration of these properties.

However, statements weren't in accordance when including the cement-based compositions. Having a higher percentage of binder content when in comparison to GP and GP.NMS, the mortars also presented lower velocities/frequencies. It could be explained by the high retraction and cracking process on the CV and CV.NMS due to the natural behaviour of PC and the claylike water release behaviour of EV. After six months of age, it was measured that a reduction of 1.5% of the specimens' dimensions due to the retraction process and cracks with a thickness thinner than 0.5mm were also visible. This set of conditions reduces the quality of the specimen. Furthermore, adding fibres does not lead to lower qualities of homogeneity, i.e., to such notorious decreased velocities/frequencies [52-54]. Also, having a lower percentage of binder, the commercial solution presented higher velocities/frequencies when compared with GV; however, this comparison isn't reliable due to the unknown content of materials of C.

It was expected that NMS would fulfil the voids, producing denser and less porous mortars [73]; however, this effect didn't occur in the gypsum based mortars as: i) GP and GP.NMS had results within a similar range of values, and ii) GV had V_p, V_s, f_f and f_t only 5%, 3%, 10% and 8% higher than GV.NMS', respectively. The statement mentioned above occurs to the cement based compositions as CV.NMS had V_p, V_s, f_f and f_t more than 11%, 7%, 16% and 15% higher than CV's, respectively. This leads to believe that NMS behaved as impurities and didn't react to the gypsum.

Table 4.3 shows the average property values from UPV and IEV tests for each mortar.

Table 4.3 – Average property results from the non-destructive tests.

Designação da Argamassa	E (GPa)	G (GPa)	μ
C	2.629	1.111	0.18
CV	0.765	0.289	0.32
CV.NMS	0.921	0.347	0.33
GP	1.286	0.526	0.23
GP.NMS	1.253	0.512	0.22
GV	2.817	1.164	0.22
GV.NMS	2.691	1.117	0.20

The Poisson's ratio directly influences the compression and flexural strengths as it is proportional to the elastic modulus of elasticity and the shear modulus (Eq. 6). In this context, several studies assessed the Poisson's ratio of cement and gypsum based mortars:

As referenced by Gercek [119], the Poisson's ratio value for pure gypsum is 0.336, and the addition of lightweight materials with lower Poisson's ratio values shall decrease it. According to Rahmanian [80], the Poisson's ratio for fire resistance gypsum materials has an average value

of 0.20. Sánchez-Aparicio *et al*. [120] reached an average Poisson's ratio value of 0.24, with a maximum of 0.32 and a minimum of 0.19. According to Zhang *et al*. [121] and Rajeev *et al*. [122], cement based mortars present an average Poisson's ratio of 0.17 with minimum and maximum values of 0.15 and 0.21. However, with an increase in water content, the mortar's Poisson's ratio also increases. CV and CV.NMS, as previously mentioned, has a high W/B ratio, thus the increased value of μ. The Poisson's ratios results of the present work are in accordance with the statements mentioned above, as seen in Table 4.3.

According to Table 4.3, it can be concluded that GV and GV.NMS group had the highest range of average E and G values. GV stands out as the composition with the highest mechanical properties values as its Young's modulus was 268%, 206%, 119%, 125% and 5% higher than CV, CV.NMS, GP.NMS, GP and GV.NMS values, respectively, and its shear modulus were 284%, 220%, 121%, 127% and 4% higher, respectively.

It is expected that the composition with the highest amount of binder also has the highest values of mechanical properties, such as the Young's modulus (E) and the shear modulus (G), due to the reduced mechanical properties values which lightweight aggregates have, as shown by several previous studies:

Gomes *et al.* [106] studied several mortars' compositions' mineralogical, mechanical and hygroscopic characteristics. The author concluded that the plain gypsum mortar had a mean Young's modulus of 4.006 GPa. Sánchez-Aparicio *et al.* [120] developed a high-fired plain gypsum mortar with Young's modulus maximum and minimum values of 4.282 and 2.211 GPa, respectively, and an average value of 2.989 GPa. By Equation 6, the mean shear modulus was equal to 1.205 GPa. Therefore, maximum and minimum values were defined for plain gypsum mortars and gypsum based mortars with lightweight aggregates.

Rahmanian [80] developed a comparative study between two gypsum panels which compositions varied from one manufacturer to another. Then, by an approximate analysis of the stress-strain relationship, E was obtained: 1.573 and 2.378 GPa for the panel with the highest content of aggregates and the lowest, respectively. As mentioned before, the Poisson's ratio obtained by this author was 0.20. Therefore, through Equation 6, the panels' shear modulus was 0.655 and 0.990 GPa, respectively.

The assessment of the means E and G showed the repetition of the phenomenon that occurred in the results from the UPV velocities and IEV frequencies in the binder content, confirming the results' reliability. Moreover, apart from the cement based composition due to the high

amount of W/B used, the results are in accordance with the literature's as the main objective of the studied mortars is to provide an enhanced thermal behaviour.

Table 4.4 summarizes the relationship between the developed mortars' and the commercial solution's mechanical parameters. Figure 4.8 shows the linear regression between E and G average values.

Table 4.4 – Developed mortars' non-destructive test results to commercial solution's ratios.

Mortar Designation	UPV's E ratios (%)	IEV's E ratios (%)	UPV's G ratios (%)	IEV's G ratios (%)
C	-	-	-	-
CV	29.1	29.0	26.0	25.9
CV.NMS	35.1	34.9	31.0	31.5
GP	44.9	53.1	43.2	51.7
GP.NMS	45.6	49.7	43.5	48.9
GV	109.7	104.6	107.7	101.8
GV.NMS	100.7	104.1	98.8	102.5

The assessment of Table 4.4 allowed to conclude that the developed mortars showed three distinct characteristics: i) CV and CV.NMS group has the lowest ratios, approximately one-third or less than the commercial solution`s results; ii) GP and GP.NMS group have E and G average values in the range of 50% lower than the commercial solution's and iii) GV and GV.NMS group showed a clear enhanced E and G average values when in comparison to C's. The enhanced results of GV and GV.NMS group are due to 75% and 74% binder content, respectively. An increase in binder content of the cement based compositions shall increase the studied properties values, as previously shown.

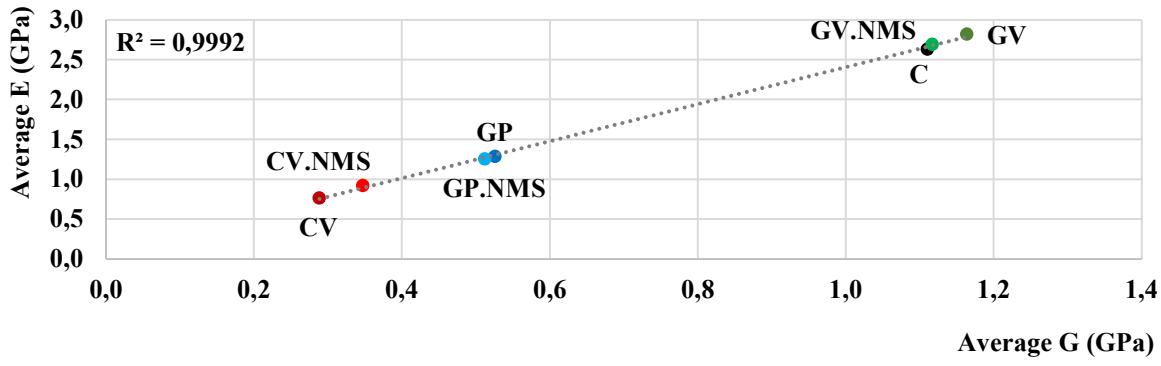

Figure 4.8 – Linear regression between the average values of the compositions' Young's modulus and shear modulus.

According to Nettleton [121], the Pearson's correlation method assigns a value between -1 and 1, where 0 means no correlation, 1 is a total positive correlation, and -1 is a total negative correlation. Based on the results of Figure 4.8, it is possible to conclude that there is a correlation between E and G since Pearson's correlation coefficient is 0.9992.

Based on this correlation, it is expected that the compositions GV, GV.NMS, C, GP.NMS, GP, CV.NMS and CV may have, respectively, the highest values of compressive and flexural strength. Next, the results of the flexural and compression tests and the respective verification of this prediction are presented.

4.3 Destructive tests

4.3.1 Flexural test

In four-support flexural tests, the flexural strength is given by the following equation:

$$f_{ct,fl} = F L / b t^2 \quad \text{(Eq. 7)}$$

where $f_{ct,fl}$ stands for the flexural strength (GPa), F for the maximum load (N), L for the distance between the lower rollers (mm), b for the width of the bar (mm) and t for the thickness of the bar (mm).

The specimens' maximum load and flexural strength values are given in Table 4.5, and the compositions' average load-displacement behaviour in the flexural test are given in Figure 4.9.

Table 4.5 – Flexural test results.

Specimen Designation	Maximum Load (N)	Average Load (N)	$f_{ct,fl}$ (MPa)	SD
C.1	984.0			
C.2	922.9	939.4	1.945	0.066
C.3	911.3			
CV.1	195.3			
CV.2	160.2	158.7	0.320	0.063
CV.3	120.6			
CV.NMS.1	442.0			
CV.NMS.2	434.6	441.2	0.913	0.011
CV.NMS.3	446.9			
GP.1	445.4			
GP.2	478.1	461.3	0.955	0.028
GP.3	460.4			

GP.NMS.1	404.1			
GP.NMS.2	445.6	419.5	0.868	0.038
GP.NMS.3	408.9			
GV.1	1065.4			
GV.2	1047.7	1057.5	2.189	0.015
GV.3	1059.3			
GV.NMS.1	979.1			
GV.NMS.2	971.4	969.8	2.008	0.017
GV.NMS.3	959.0			

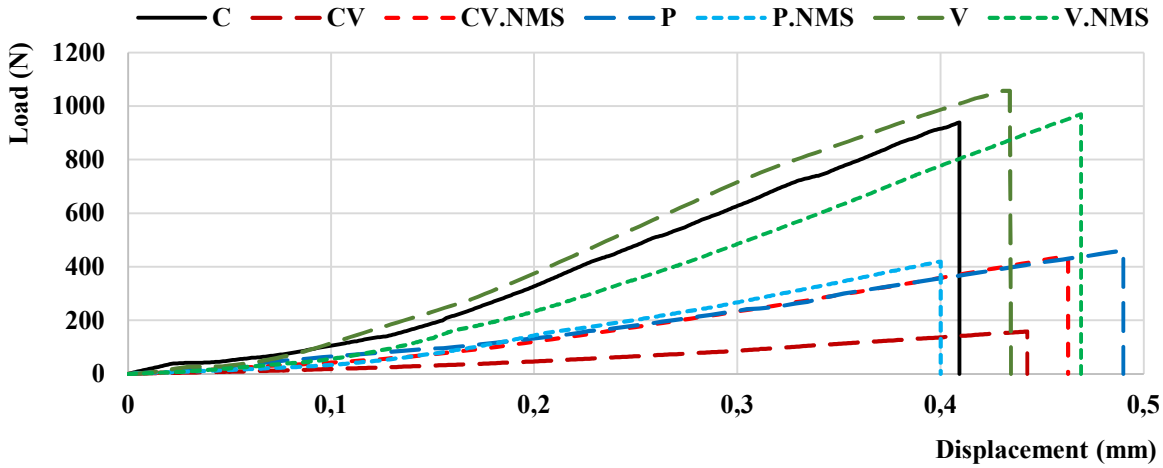

Figure 4.9 – Flexural tests' load-displacement curves.

4.3.2 Compression test

Such as the flexural test procedure, when the specimen's collapse occurred, the maximum load was registered. The compression strength is given by the following equation:

$$f_{ct,c} = F / d^2 \quad \text{(Eq. 8)}$$

where $f_{ct,c}$ stands for the compression strength (GPa), F for the maximum load (N), and d for the dimension of the piston's square section steel plate (mm).

The specimens' maximum load and compression strength values are given in Table 4.6, and the compositions' average load-displacement behaviour in the compression test are given in Figure 4.10.

Table 4.6 – Compression test results.

Specimen Designation	Maximum Load (N)	Average Load (N)	$f_{ct,c}$ (MPa)	SD
C.1.1	5259.0			
C.1.2	5306.1	5275.2	3.297	0.013
C.2.1	5260.5			
CV.1.1	965.5			
CV.1.2	738.5	863.5	0.540	0.059
CV.2.1	886.5			
CV.NMS.1.1	2322.6			
CV.NMS.1.2	2335.3	2345.4	1.466	0.015
CV.NMS.2.1	2378.2			
GP.1.1	1628.0			
GP.1.1	1575.4	1636.6	1.023	0.034
GP.2.1	1706.4			
GP.NMS.1.1	1833.9			
GP.NMS.1.2	1711.7	1775.9	1.110	0.050
GP.NMS.2.1	1782.1			
GV.1.1	5040.3			
GV.1.2	4937.9	5007.5	3.139	0.031
GV.2.1	5044.3			
GV.NMS.1.1	4387.8			
GV.NMS.1.2	4552.7	4427.5	2.767	0.091
GV.NMS.2.1	4341.9			

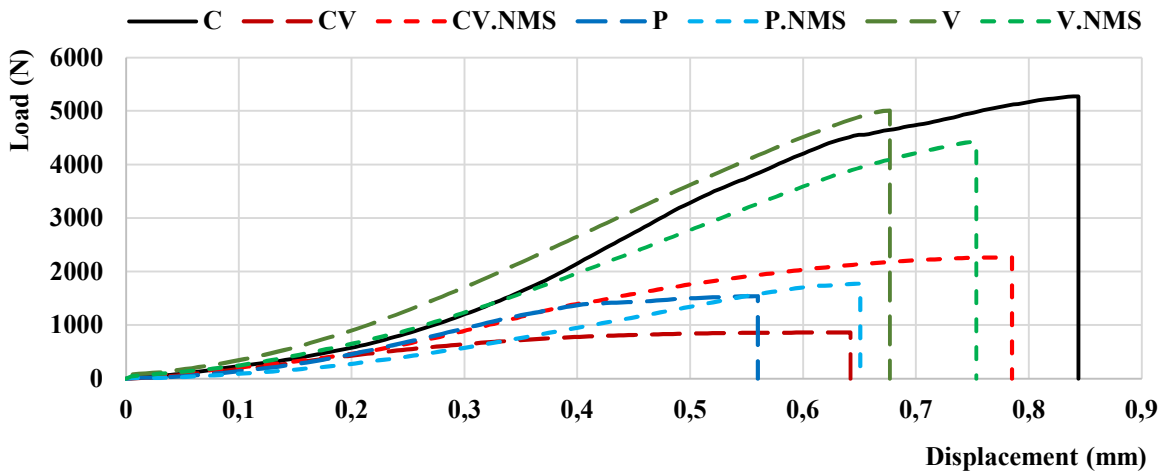

Figure 4.10 – Compression tests' load-displacement curves.

4.3.3 Discussion of the tests results

The assessment of the developed mortars' destructive test results allowed observing a decrease in flexural and compression strengths when higher amounts of aggregate are added. Therefore, plain mortars tend to have higher strengths than lightweight mortars.

Several studies defined a range of values for plain cement and gypsum mortars. However, the strengths values are highly dependent on the amount of water content [122]:

The gypsum based mortars studied by Gomes *et al.* [106] were submitted to flexural and compressive tests, and their average values were 1.51 and 4.15 MPa, respectively. Sánchez-Aparicio *et al.* [120] also obtained compressive strength results from the previous study: by a stress-strain test procedure, the values were in a range of 3.57 to 4.53 MPa with an average value of 4.01 MPa. Babu *et al.* [123] obtained, for the plain gypsum reference mortar, flexural and compressive strengths of 2.48 and 4.75 MPa, respectively.

According to Mo *et al.* [76], the water to cement ratio is directly correlated to the specimen's compression strength as, at room temperature, the 0.52 W/B specimen had a compression strength of 33.03 MPa, 140% higher than the 0.71 W/B specimen's strength. Benli *et al.* [124] concluded that, at 90 days of age, the 0.41 W/B cement based specimen had flexural and compressions strengths of 11.34 and 78.21 MPa. Moreover, an increment in the content of water drastically reduces the strengths. Köksal *et al.* [125] studied the flexural and compression strengths of several insulating mortars, and the 0.5 W/B control cement based specimen had average values of 48.3 and 6.6 MPa, respectively. The compositions of the before-mentioned specimens were only constituted by cement, sand and water, thus, with high strengths values. The results highlight the importance and influence of the water to binder ratio and the reduced flexural strengths that cement based compositions have compared to the compression strengths.

As previously mentioned, expanded perlite and vermiculite's main objective is to provide an improved thermal behaviour to the mortars [19]; hence, weaker aggregates lead to lower resistance, reducing the load-bearing capacity of the mortars. From previous studies, it was seen that the usage of insulating aggregates reduces the mortar's compressive and the flexural strengths:

Mo *et al.* [76] concluded that the incorporation of lightweight aggregates in mortars decreased its mechanical strength: by compression tests' results, it was possible to see that the reference mortar had strength 99% higher than the composition with less amount of aggregate and 173%

higher than the composition with the highest amount. According to Köksal *et al*. [83], samples with smaller quantities of vermiculite present enhanced strengths as the V/B = 4 mortar had flexural and compressive strengths 10% and 100% higher, respectively, than the V/B = 8 mortar's. The author also studied the usage of this aggregate in others compositions [84] and concluded that the composition with the smallest amount of vermiculite had a compressive strength 108% higher than the one with the highest amount of the aggregate.

The literature review agrees with the developed compositions' results, as the highest mechanical strengths are observed in the GV and GV.NMS group which have 25% and 24%, respectively, of aggregate content, while the GP and GP.NMS group have 50% and 49%, respectively. Due to the high water to binder content, CV and CV.NMS group presents lower strengths compared with the literature's cement based mortars.

Moreover, it is observed that the addition of nano and micro silica particles achieved the expected effect when added to the cement based mortar [60-73]. However, it is observed that the addition of nano and micro silica particles caused a decrease in the flexural strength and a slight variation in GP and GP.NMS group's compression strength and a decrease in GV and GV.NMS group's compression strength.

Table 4.7 summarizes each mortar's strengths and the relationship between the developed mortars' and the commercial solution's strengths.

Table 4.7 – Developed mortars' destructive test results and comparison ratios to the commercial solution's.

Specimen Designation	**Flexural Strength (MPa)**	**Flexural Strength *versus* C's (%)**	**Compression Strength (MPa)**	**Compression Strength *versus* C's (%)**
C	1.945	-	3.297	-
CV	0.320	16.5	0.540	16.4
CV.NMS	0.913	46.9	1.466	44.5
GP	0.955	49.1	1.023	31.0
GP.NMS	0.868	44.6	1.110	33.7
GV	2.189	112.5	3.139	95.2
GV.NMS	2.008	103.2	2.767	83.9

Showing the best performance between the developed mortars, GV had flexural and compressive strengths 584% and 481% higher than CV's, 140% and 114% higher than CV.NMS', 9% and 13% higher than GV.NMS', 129% and 206% higher than GP's and 152% and 182% higher than GP.NMS', respectively. When comparing the commercial composition

with the developed mortars, GV and GV.NMS group had enhanced flexural strengths and decreased compression strengths; however, the results are within a similar range of values.

The results shown in Table 4.7 are in accordance with the non-destructive test results, as the highest velocities/frequencies are seen in GV and the lowest in CV.

C and GV stand out as the compositions with the best mechanical behaviours; however, passive fire protection mortars' mechanical strengths aren't limited by a minimum value, according to Ref. [124]. Hence, only thermal requirements should have complied with.

To obtain the magnitude of the reliability of the data, several linear approaches of the different test results are seen in Figure 4.11.

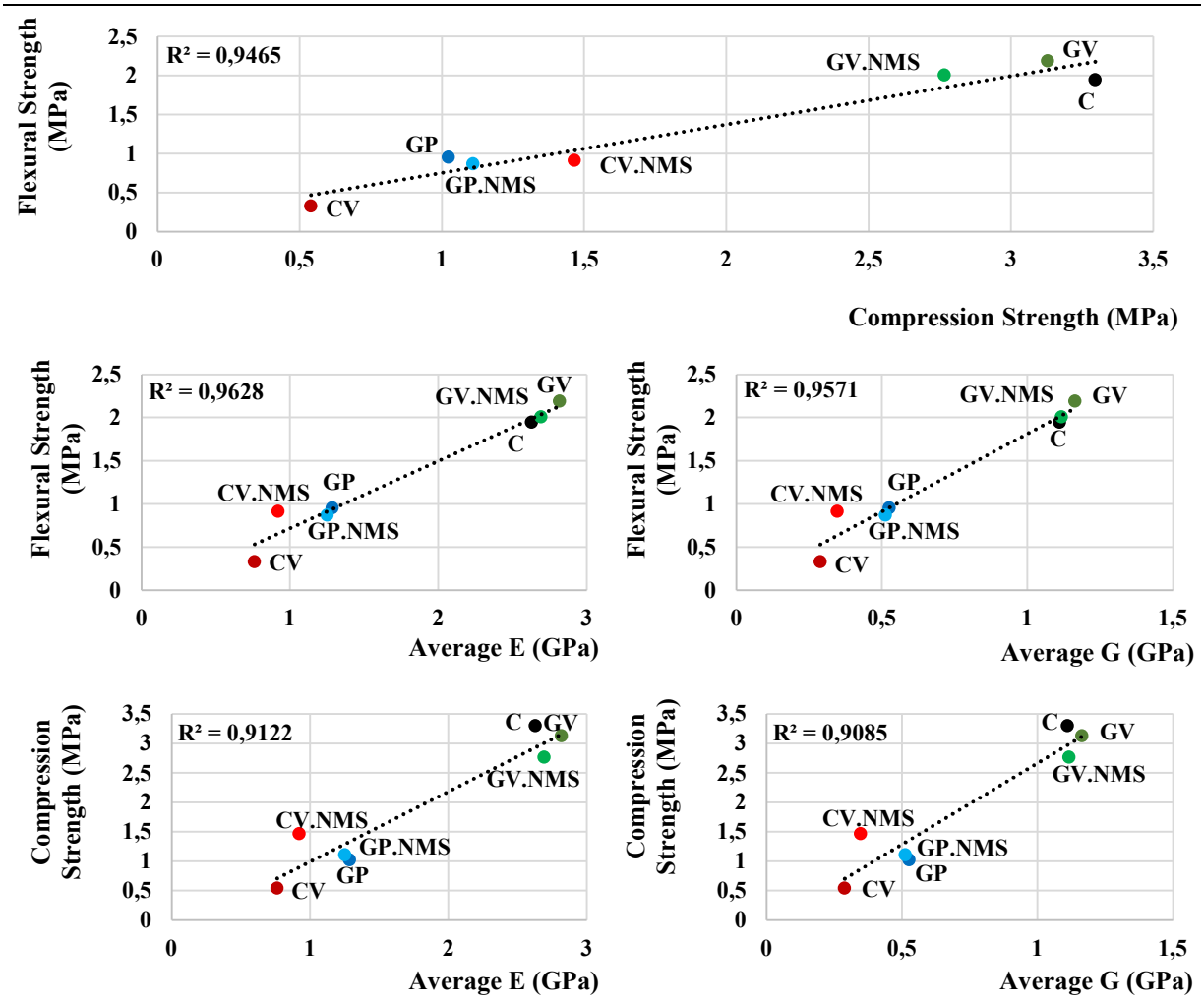

Figure 4.11 – Studied mortars' mechanical parameters' linear regression relationship.

From Figure 4.11, it is observed that the flexural strength is highly correlated to the mortars' Young's modulus and shear modulus as the Pearson's factors are 0.963 and 0.957. It is also verified that there is a strong correlation between the compressive strength of the various mortars and the respective Young´s modulus of elasticity and shear modulus, namely, 0.912 and 0.909, respectively. Although the correlation between flexural strength versus compressive strength is not as high as the previous ones, a correlation of 0.947 can be identified. These correlation factors are also in accordance with the exposed by Nettleton [121].

Moreover, excluding CV and CV.NMS group, due to the affected results by the elevated water to binder ratio used, the correlation factors increased:

Flexural *vs* compression strengths	$R^2 =$ 0.943
Flexural strength *vs* average E	$R^2 =$ 0.995
Flexural strength *vs* average G	$R^2 =$ 0.992
Compression strength *vs* average E	$R^2 =$ 0.958
Compression strength *vs* average G	$R^2 =$ 0.967

5 CONCLUSIONS AND FUTURE WORKS

The objective of this work was the mechanical characterization of cement and gypsum based mortars for passive fire protection. Seven types of compositions, among one commercial solution, were tested to evaluate the influence of the amount of binder and aggregates and the effects of the addition of nano and micro silica particles on the mechanical behaviour of the mortars by non-destructive and destructive tests. Moreover, complementary tests were carried out to proceed with the physical characterization of the specimens. The following conclusions can be taken from the results of this work:

- The results of the complementary tests concluded that the better thermal performance of the GP.NMS composition, when compared to C, is due to the fact that it loses less mass with increasing temperature (consequently, less cracking) and due to the existence of an amorphous material (EP) in its composition.

- From the analysis of the non-destructive tests, it is concluded that the mortars developed have uniform, and homogeneous matrices since the values of velocities/frequencies are in agreement with the range of values presented in the review literature.

- It was also concluded that the higher the binder dosage and the lower the aggregate dosage, the higher the velocities/frequencies obtained in the non-destructive tests and, consequently, higher values of mechanical strength and physical properties.

  It was concluded that the compositions GV and GV.NMS presented superior or similar mechanical properties to the commercial composition and the CV, CV.NMS, GP and GP.NMS presented inferior mechanical properties to the commercial composition.

- Adding 1% by volume of nano and micro silica particles in the mortars developed in the laboratory (CV, CV.NSM, GP, GP.NMS, GV and GV.NMS) improved their thermal properties (thermal conductivity and specific heat). However, its addition into the gypsum based mortars caused a decrease in its mechanical and physical properties, namely, flexural and compression strength, Young's modulus elasticity, shear modulus and Poisson's ratio.

- The addition of NMS into the cement based composition showed the expected effectiveness, as it was more homogeneous and had higher strengths than CV.

- It was concluded that for the mortars developed, the mechanical properties studied (flexural and compression strength) seems to be well correlated with the physical properties (Young's modulus and shear modulus) since the correlation values vary between 0.909 and 0.963.

In the context of the presented work, it will be proposed several future works which could minimize the problems and gaps found during this research:

- It was clear the effects of cracking of the cement bases mortars; however, the addition of glass fibres into the compositions with polypropylene fibres shall enhance both thermal and mechanical behaviour of the mortars. In this context, a study within this scope shall be defined.

- The addition of a higher amount of nano and micro silica particles into the gypsum based compositions shall be an object of study to understand if the NMS behaves as impurities or the content of 1% in volume was insufficient.

- The mechanical characterization by static non-destructive tests shall be done in future work to characterize the mortars' Young's modulus' curve completely. It's important to refer that the dynamic tests are reliable; however, if commercialized, it's relevant to the Young's modulus curve to be characterized.

- It is important to study the expenses of fabrication of the developed mortars. It is clear that GV and GV.NMS shows the highest strength values when in comparison to the developed mortars and similar values when in comparison to the commercial solution. However, the objective of the Nanofire project is to develop passive fire protection mortars, i.e., mortars with enhanced thermal behaviour, therefore, not only GV and GV.NMS but all mortars shall be an objective of analyses of cost study. The developed mortar's expenses shall decrease if developed in large scale production [126-127]. In this context, the study of large-scale production of GP.NMS and GV shall be an objective of the study to understand the viability of commerciality.

- A study of the application procedure of the developed mortars to the steel structure shall be done. A sprayed solution seems to be the most indicated method [7].

REFERENCES

[1] Gervásio, H., L., Simoes da Silva., Bragança, L., (2005), "Sustainability assessment of new construction technologies: a comparative case study", COST C12 Final Conference Proceedings, Balkema, Leiden, 527-536.

[2] Eckelman, M.J., Brown, C., Troup, L.N., Wang, L., Webster, M.D., Hajjar, J.F., (2018), "Life cycle energy and environmental benefits of novel design-for-deconstruction structural systems in steel buildings", Building and Environment, 143, 421-430, doi.org/10.1016/j.buildenv.2018.07.017.

[3] Shi, G., Ban, H., Shi, Y., Wang, Y., (2012), "Overview of research progress for high strength steel structures", Engineering Mechanics, Vol. 30, No.1, doi.10.6052/j.issn.1000-4750.2012.05.ST10.

[4] Gervásio, H. e Simões da Silva, L. (2005). "A sustentabilidade do aço", Construção Metálica e Mista V, CMM, Lisboa, 719-730.

[5] Santiago, A., Simões da Silva, L., Vaz, G., Vila Real, P., Gameiro Lopes, A., (2008), "Experimental investigation of the behaviour of a steel sub-frame under a natural fire", International Journal of Steel and Composite Structures 8(3), 243-264, doi.10.12989/scs.2008.8.3.243.

[6] Ryou, J., Kim, H., (2017), "New approach for delaying the internal temperature rise of fire resistant mortar made with coated aggregate", Construction and Building Materials, 149, 76–90, doi.org/10.1016/j.conbuildmat.2017.05.116.

[7] Vilches, L.F., Leiva, C., Olivares, J., Vale, J., Fernández, C., (2005), "Coal fly ash-containing sprayed mortar for passive fire protection of steel sections", MATER CONSTRUCC, Vol. 55, nº 278.

[8] Couto, C., Real, P.V., (2021), "The influence of imperfections in the critical temperature of I-section steel members", Journal of Constructional Steel Research, 179, 106540, doi.org/10.1016/j.jcsr.2021.106540.

[9] Laím, L., Santiago, A., Caetano, H., Craveiro, H.D., Shahbazian, A., (2022), "Numerical analysis and structural fire design of protected SHS steel columns with thermally enhanced gypsum-based mortars", Journal of Building Engineering, 54, 104629, doi.org/10.1016/j.jobe.2022.104629.

[10] Hager, I., Mróz, K., Korniejenko, K., (2016), "Material solutions for passive fire protection of buildings and structures and their performances testing", Procedia Engineering, 151, 284 – 291, doi.10.1016/j.proeng.2016.07.388.

[11] Forell, B., Peschke, J., Einarsson, S., Röwekamp, M., (2016), "Technical reliability of active fire protection features – generic database derived from German nuclear power plants", Reliability Engineering and System Safety, 145, 277–286,

doi.org/10.1016/j.ress.2015.09.010.

[12] Lima, G.P.A., Barbosa, J.D.V., Beal, V.E., Gonçalves, M.A.M.S, Machado, B.A.S., Gerber, J.Z., Lazarus, B.S., (2021), "Exploratory analysis of fire statistical data and prospective study applied to security and protection systems", International Journal of Disaster Risk Reduction, 61, 102308, doi.org/10.1016/j.ijdrr.2021.102308.

[13] Bradley, I., Wiloughby, D., Royle, M., (2019), "A review of the applicability of the jet fire resistance test of passive fire protection materials to a range of release scenarios", Process Safety and Environmental Protection, 122, 185–191, doi.org/10.1016/j.psep.2018.12.004.

[14] Landucci, G., Rossi, F., Nicolella, C., Zanelli, S., (2009), "Design and testing of innovative materials for passive fire protection", Fire Safety Journal, 44, 1103-1109, doi.10.1016/j.firesaf.2009.08.004.

[15] Tomar, M.S., Khurana, S., (2019), "Impact of passive fire protection on heat release rates in road tunnel fire: A review", Tunnelling and Underground Space Technology, 85, 149 – 159, doi.org/10.1016/j.tust.2018.12.018.

[16] Milke, J., (2016), "Fire protection as the underpinning of good process safety programs", Journal of Loss Prevention in the Process Industries, 40, 329 – 333, doi.org/10.1016/j.jlp.2015.11.021.

[17] EN 1993-1-2-2005, (2005), "Eurocode 3: Design of Steel Structures. Part 1.2: General Rules – Structural fire design", European Committee for Standardization – CEN. EN 1993-1-2-2005.

[18] Formosa J., Chimenos J.M., Lacasta A.M., Haurie L., Rosell J.R., (2010), "Novel fire-protecting mortars formulated with magnesium by-products", doi.org/10.1016/j.cemconres.2010.11.009.

[19] Caetano, H., Laím, L., Santiago A., Durães L. and Shahbazian A., (2022), "Development of Passive Fire Protection Mortars", Applied Sciences, DPI 12, 2093.

[20] EN 1993-1-1-2005, (2005), "Eurocode 3: Design of Steel Structures. Part 1.1: General Rules and Rules for Buildings", European Committee for Standardization – CEN. EN 1993-1-1-2005.

[21] Juhás, P., Šenitková, I.J., (2006), "Strength and Resistance of Structural Steels and Materials", Materials Science and Engineering, doi.10.1088/1757-899X/1066/1/012006.

[22] Jordão, S., Simões da Silva, L., Simões, R., (2014), "Design formulation analysis for high strength steel welded beam-to-column joints", Engineering Structures, 70, 63-81, dx.doi.org/10.1016/j.engstruct.2014.02.028.

[23] Simões, R., Jordão, S., Diogo, J., Fernandes, J., (2017), "Development and design of a concealed splice joint configuration between tubular sections", Engineering Structures, 137, 181-193, dx.doi.org/10.1016/j.engstruct.2017.01.054

[24] Johansson, B., Collin, P., "Eurocode for High Strength Steel and Applications in Construction"

[25] Baetu, G., Galatanu, T., Baetu, S., (2017), "Behaviour of Steel Structures under Elevated Temperature", Procedia Engineering, 181, 265-272, doi.10.1016/j.proeng.2017.02.388.
[26] Bhanuse, M.M., Jankar, P.D., (2013), "Behaviour of Steel under Elevated Temperature-Experimental work", Internation Journal of Advanced Scientific and Technical Research, Vol. 6, ISSN 2249-9954.
[27] Laím, L., Craveiro, H.D., Simões, R., Escudeiro, A., Mota, A., (2020), "Experimental analysis of cold-formed steel columns with intermediate and edge stiffeners in fire", Thim-Walled Structures, 146, 106481, doi.org/10.1016/j.tws.2019.106481.
[28] Sun, J., Nitschke-Pagel, T., Dilger, (2021), "Influence of temperature- and phase-dependent yield strength on residual stresses in ultra-high strength steel S960 weldments", Journal of Materials Research and Technology, 15, 1854-1872.
[29] Randaxhe, J., Popa, N., Vassarat, O., Tondini, N., (2021), "Development of a plug-and-play fire protection system for steel columns", Fire Safety Journal, 121, 103272, doi.org/10.1016/j.firesaf.2020.103272.
[30] EN 1990, (2009), "Eurocode: Basic of structural design", European Committee for Standardization – CEN. EN 1993-1-1-2009.
[31] Diário da República, 1.ª série, Ministério da Administraçao Interna, Decreto-Lei n.º 220/2008, 12 de novembro.
[32] Diário da República, 1.ª série, Ministério da Administraçao Interna, Portaria n.º 1532/2008, 29 de dezembro.
[33] Santiago, A., (2008), "Behaviour of Beam-to-Column Steel Joints Under Natural Fire", University of Coimbra.
[34] Iqbal, S., Harichandran, R.S., (2011), "Capacity reduction and fire load factors for LRFD of steel columns exposed to fire", Fire Safety Journal, 46, 234-242.
[35] Council Directive 89/106/EEC, (1993), "The Construction Products Directive", 22 july.
[36] Li, G., Lou, G., Zhang, C., Wang, L., Wang, Y., (2012), "Assess the Fire Resistance of Intumescent Coatings by Equivalent Constant Thermal Resistance", Fire Technology, 48, 529-546, doi.10.1007/s10694-011-0243-8.
[37] Bourbigot, S., Duquesne, S., Leroy, J., (1999), "Modeling of Heat Transfer of a Polypropylene-Based Intumescent System during Combustion", Journal of Fire Sciences, vol. 17.
[38] Khana, A.S., Puri, R.G., (2016), "Intumescent coatings: A review on recent progress", J. Coat. Technology Res., doi.10.1007/s11998-016-9815-3.
[39] Islam, Md. M., Ali, R.B., (2018), "Fire Protection of Steel Structure: An Overall Review", World Scientific News, EISSN 2392-2192
[40] Internet gate, geradordeprecos.info/obra_nova/Instalacoes/Contra_incendios/IOR_Proteccao_passiva_contra_incen/IOR040_Proteccao_passiva_contra_incendios_.html
[41] Internet gate, titantech.pt/pt/produtos/ix-085-tinta-intumescente-a85
[42] Internet gate, aecweb.com.br/revista/materias/pintura-intumescente-em-estrutura-metalica-pede-mao-de-obra-qualificada/17296

[43] Internet gate, tratamentoacustico.com.br/protecao-passiva-contra-fogo/pintura-intumescente/
[44] Li, G., Jiang, S., (1999), "Prediction to nonlinear behaviour of steel frames subjected to fire", Fire Safety Journal, 32, 347-368.
[45] Internet gate, isopur.com.br/la-de-rocha/la-de-rocha-com-felt.html
[46] Internet gate, casaeconstrucao.org/materiais/la-de-vidro/
[47] Wakili, K.G., Hugi, E., Wullschleger, L., Frank, Th., (2007), "Gypsum Board in Fire – Modeling and Experimental Validation", Journal of Fire Sciences, Vol. 25, doi:10.1177/0734904107072883.
[48] Usamani, A.S., Rotter, J.M., Lamont, S., Sanad, A.M., Gillie, M., (2001), "Fundamental principles of structural behaviour under thermal effects", Fire Safety Journal, 36, 721-744.
[49] Internet gate, promat.com/en-hk/construction/projects/expert-area/
[50] Internet gate, envirograf.com/product/board-for-protection-of-steel/
[51] Internet gate, ribaj.com/products/promat-real-world-tested-fire-protection-board
[52] Li, L., Gao, D., Li, Z., Cao, M., Gao, J., Zhang, Z., (2020), "Effect of high temperature on morphologies of fibres and mechanical properties of multi-scale fibre reinforced cement-based composites", Construction and Building Materials, 261, 120487, doi.org/10.1016/j.conbuildmat.2020.120487.
[53] Mohammed, E., Molez, L., Jauberthie, R., Rangeard, D., (2011), "Heat exposure tests on various types of fibre mortar", European Journal of Environmental and Civil Engineering, dx.doi.org/10.1080/19648189.2011.9693360.
[54] Mohammed, E., Kadri, T., Molez, L., Jauberthie, R., Balhacen, A., (2015), "High temperature behaviour of polypropylene fibres reinforced mortars", Fire Safety Journal, 71, 324-331, doi.10.1016/j.firesaf.2014.11.022.
[55] Internet gate, vivablast.com/our-services/passive-fire-protection/
[56] Internet gate, iriscoatings.it/fireproofing-mortars.
[57] Abidi, S., Nait-Ali, B., Joliff, Y., Favotto, C., (2014), "Impact of perlite, vermiculite and cement on the thermal conductivity of a plaster composite material: Experimental and numerical approaches", Composites: Part B, 68, 392–400, doi.org/10.1016/j.compositesb.2014.07.030.
[58] Janica, I., Del Buffa, S., Mikotajczak, A., Eredia, M., Pakulski, D., Ciesielski, A., Samorì, P., (2018), "Thermal insulation with 2D materials: liquid phase exfoliated vermiculite functional nanosheets", Nanoscale, 10 23182–23190, doi:10.1039/c8nr08364a.
[59] Rodrigues, J.P.C., Caetano, H., Ferreira, G., Pimienta, P., (2019), "Temperature Effect On The Concrete Microstructure And Its Influence On The Compressive Strength", Construction and Building Materials, vol. 199, 717-736, doi.org/10.1016/j.conbuildmat.2018.12.074.

[60] Horszczaruk, E., Sikora, P., Horszczaruk, K., Mijowska, E., (2017), "The effect of elevated temperature on the properties of cement mortars containing nanosilica and heavyweight aggregates", Construction and Building Materials, 137, 420–431, doi.org/10.1016/j.conbuildmat.2017.02.003.

[61] Mijowska, E., Horszczaruk, E., Sikora, P., Cendrowski, K., (2018), "The effect of nanomaterials on thermal resistance of cement-based composites exposed to elevated temperature", Materials Today: Proceedings, 5, 15968–15975.

[62] Hou, P., Kawashima, S., Wang, K., Corr, D.J., Quian, J., Shah, S.P., (2012), "Effects of colloidal nanosilica on rheological and mechanical properties of fly ash–cement mortar", Cement & Concrete Composites, 35, 12–22, doi.org/10.1016/j.cemconcomp.2012.08.027.

[63] Nuaklong, P., Boonchoo, N., Jongvivatsakul, P., Charinpanitkul, T., Sukontasukkul, P., (2020), "Hybrid effect of carbon nanotubes and polypropylene fibres on mechanical properties and fire resistance of cement mortar", Construction and Building Materials, 275, 122189, doi.org/10.1016/j.conbuildmat.2020.122189.

[64] Polat, R., Quarluq, A.W., Karagöl, F., (2021), "Influence of singular and binary nanomaterials on the physical, mechanical and durability properties of mortars subjected to elevated temperatures and freeze–thaw cycles", Construction and Building Materials, 295, 123608, doi.org/10.1016/j.conbuildmat.2021.123608.

[65] Irshidat, M., Al-Saleh, M.H., (2017), "Thermal performance and fire resistance of nanoclay modified cementitious materials", Construction and Building Materials, 159, 213–219, doi.org/10.1016/j.conbuildmat.2017.10.127.

[66] Gomes, M.G., Flores-Colen, I., Pedroso, M., (2018), "Thermal conductivity measurement of thermal insulating mortars with EPS and silica aerogel by steady-state and transient methods", Construction and Building Materials, 172, 696–705, doi.org/10.1016/j.conbuildmat.2018.03.162.

[67] Jindal, B.B., Sharma, R., (2020), "The effect of nanomaterials on properties of geopolymers derived from industrial by-products: A state-of-the-art review", Construction and Building Materials, 252, 119028, doi.org/10.1016/j.conbuildmat.2020.119028.

[68] Nalon, G.H., Ribeiro, J.C.L, Araújo, E.N.D., Pedroti, L.G., Carvallho, J.M.F, Santos, R.F., Oliveira, D.S., (2021), "Residual mechanical properties of mortars containing carbon nanomaterials exposed to high temperatures", Construction and Building Materials, 275, 122123, doi.org/10.1016/j.conbuildmat.2020.122123.

[69] Ibrahim, R.Kh., Hamid, R., Taha, M.R., (2012), "Fire resistance of high-volume fly ash mortars with nanosilica addition", Construction and Building Materials, 36, 779–786, doi.org/10.1016/j.conbuildmat.2012.05.028.

[70] Rashad, A.M., (2013), "Effects of ZnO2, ZrO2, Cu2O3, CuO, CaCO3, SF, FA, cement and geothermal silica waste nanoparticles on properties of cementitious materials – A short guide for Civil Engineer", Construction and Building Materials, 48, 1120–1133,

doi.org/10.1016/j.conbuildmat.2013.06.083.

[71] Farzadnia, N., Ali, A.A.A., Demirboga, R., Anwar, M.P., (2013), "Effect of halloysite nanoclay on mechanical properties, thermal behaviour and microstructure of cement mortars", Cement and Concrete Research, 48, 97–104, doi.org/10.1016/j.cemconres.2013.03.005.

[72] Oltulu, M., Şahin, R., (2012), "Effect of nano-SiO2, nano-Al2O3 and nano-Fe2O3 powders on compressive strengths and capillary water absorption of cement mortar containing fly ash: A comparative study", Energy and Buildings, 58, 292–301, doi.org/10.1016/j.enbuild.2012.12.014.

[73] Laím, L., Caetano, H., Santiago, A., (2020), "Review: Effects of nanoparticles in cementitious construction materials at ambient and high temperatures", Journal of Building Engineering, doi.org/10.1016/j.jobe.2020.102008.

[74] Coniglio, M., Longstaffe, F.J., Hardie, L.A., Church, M., (2003), "Encyclopedia of sediments and sedimentary rocks", 675-676, doi.org/10.1007/978-1-4020-3609-5.

[75] Papadopoulos, A.P., Bar-Tal, A., Silber, A., Saha, U.K., Raviv, M., (2008), "Inorganic and synthetic organic components of soilless culture and potting mixes", Chapter 12, 511-512, doi.org/10.1016/B978-044452975-6.50014-9.

[76] Mo, K.H., Lee, H.J., Liu, M.Y.J, Ling, T., (2018), "Incorporation of expanded vermiculite lightweight aggregate in cement mortar", Construction and Building Materials, 179, 302–306, doi.org/10.1016/j.conbuildmat.2018.05.219.

[77] Lushnikova, N., Dvorkin, L., (2016), "Sustainability of gypsum products as a construction material", Sustainability of Construction Materials, doi.org/10.1016/B978-0-08-100370-1.00025-1.

[78] Karni, K., Karni, E., (1995), "Gypsum in construction: origin and properties", Materials Structures, 28, 92–100, doi.org/10.1007/BF02473176.

[79] Freire, M.T., Santos Silva, A., M.R., Veiga, J. Brito, (2018), "Studies in ancient gypsum based plasters towards their repair: Mineralogy and microstructure", Construction Building Materials, 196, 512-529, doi.org/10.1016/j.conbuildmat.2018.11.037.

[80] Rahmanian, I., (2011), "Thermal and mechanical properties of gypsum boards and their influences on fire resistance of gypsum board based systems", University of Manchester.

[81] Kondratieva, N., Barre, M., Goutenoire, F., Sanytsky, M., (2017), "Study of modified gypsum binder", Construction and Building Materials, 149, 535-542, doi.org/10.1016/j.conbuildmat.2017.05.140.

[82] Monteiro, P.J.M., Mehta, P.K., (2014), "Concrete: Microstructure, Properties, and Materials", Fourth Edition, ISBN: 978-0-07-179788-7.

[83] Köksal, F., Serrano-López, M.A., Şahin, M., Gencel, O., López-Colina, C., (2014), "Combined effect of steel fibre and expanded vermiculite on properties of lightweight mortar at elevated temperatures", Materials and Structures, doi.org/10.1617/s11527-014-0294-7.

[84] Köksal, F., Gencel, O., Kaya, M., (2015), "Combined effect of silica fume and expanded vermiculite on properties of lightweight mortars at ambient and elevated temperatures", Construction and Building Materials, 88, 175–187, doi.org/10.1016/j.conbuildmat.2015.04.021.

[85] Gencel, O., Gholampour, A., Tokay, H., Ozbakkaloglu, T., (2021), "Replacement of Natural Sand with Expanded Vermiculite in Fly Ash-Based Geopolymer Mortars", Appl. Sci., 11, 1917, doi.org/10.3390/app11041917.

[86] Hasanabadi, S., Sadrameli, S.M., Sami, S., (2020), "Preparation, characterization and thermal properties of surface-modified expanded perlite/paraffin as a form-stable phase change composite in concrete", Journal of Thermal Analysis and Calorimetry, doi.org/10.1007/s10973-020-09440-1.

[87] ElNemr, A., (2020), "Generating water/binder ratio -to- strength curves for cement mortar used in Masonry walls", Construction and Building Materials, 233, 117249, doi.org/10.1016/j.conbuildmat.2019.117249.

[88] Vaz-Ramos, J., Santiago, A., Portugal, A., Durães, L., (2019), "Synthesis of silica nanoparticles to enhance the fire resistance of cement mortars", Fire Research, 3, 44–48, doi:10.4081/fire.2019.77.

[89] ASTM D 2845-05, (2005), "Standard Test Method for Laboratory Determination of Pulse Velocities and Ultrasonic Elastic Constants of Rock".

[90] ASTM E 1876-01, (2002), "Standard Test Method for Dynamic Young's Modulus, Shear Modulus, and Poisson's Ratio by Impulse Excitation of Vibration".

[91] EN 12390-5, (2019), "Testing hardened concrete. Part 5: Flexural strength of test specimens".

[92] EN 1015, (2020), "Methods of test for mortar for masonry. Part 11: Determination of flexural and compressive strength of hardened mortar".

[93] Grandjean, S., Absi, J., Smith, D.S., (2005), "Numerical calculations of the thermal conductivity of porous ceramics based on micrographs", Journal of the European Ceramic Society, 26, 2669–2676, doi.10.1016/j.jeurceramsoc.2005.07.061.

[94] Ramírez, C.P., Barriguete, A.V., Somolinos, R.S., Merino, M.R, Sánchez, E.A., (2020), "Analysis of fire resistance of cement mortars with mineral wool from recycling", Construction and Building Materials, 265, 120349, doi.org/10.1016/j.conbuildmat.2020.120349.

[95] Koksal, F., Mutluay, E., Gencel, O., (2019), "Characteristics of isolation mortars produced with expanded vermiculite and waste expanded polystyrene", Construction and Building Materials, 236, 117789, doi.org/10.1016/j.conbuildmat.2019.117789.

[96] Formosa, J., Haurie, L., Chimenos, J.M., Lacasta, A.M., Rosell, J.R., (2008), "Comparative Study of Magnesium By-Products and Vermiculite Formulations to Obtain Fire Resistant Mortars", Materials Science Forum, Vols 587-588, 898-902, doi.org/10.4028/www.scientific.net/MSF.587-588.898.

[97] Vilches, L.F., Fernández-Pereira, C., Valle, J.O., Rodríguez-Piñero, Vale, J., (2002),

"Development of new fire-proof products made from coal fly ash: the CEFYR Project", Journal of Chemical and Technology and Biotechnology, 77:361-366, doi:10.1002/jctb.592.

[98] Leiva, C., Vilches, L.F., Vale, J., Olivaress, J., Fernández-Pereira, C., (2008), "Effect of carbonaceous matter contents on the fire resistance and mechanical properties of coal fly ash enriched mortars", Fuel, 87, 2977–2982, doi:10.1016/j.fuel.2008.04.020.

[99] Hager, I., Sitarz, M., Mróz, K., (2021), "Fly-ash based geopolymer mortar for high-temperature application – Effect of slag addition", Journal of Cleaner Production, 316, 128168, doi.org/10.1016/j.jclepro.2021.128168.

[100] Ezziane, M., Molez, L., Jauberthie, R., Rangeard, D., (2011), "Heat exposure tests on various types of fibre mortar", European Journal of Environmental and Civil Engineering, doi.org/10.1080/19648189.2011.9693360.

[101] ASTM C20-00, (2010), "Standard Test Methods for Apparent Porosity, Water Absorption, Apparent Specific Gravity, and Bulk Density of Burned Refractory Brick and Shapes by Boiling Water".

[102] ISO/DIS 15901-1, (2014), "Evaluation of pore size distribution and porosity of solid materials by mercury porosimetry and gas adsorption, Part 1: Mercury porosimetry".

[103] Ugarte, J.F.O, Sampaio, J.A., França, S.C.A., (2008), "Industrial Rocks and Minerals. Chapter 38: Vermiculite", CETEM, 2º Edition.

[104] Filho, S.H.S, Vinaches, P., Pergher, S.B.C., (2017), "Structural characterization of expanded perlite", PERSPECTIVA, Erechim, Vol. 41, 155, 81-87.

[105] EN 1991-1-1-2009, (2009), "Eurocode 1: Actions on Structures. Part 1.1: General Actions ", European Committee for Standardization – CEN. EN 1993-1-1-2009.

[106] Azdarpour, A., Karaei, M.A., Hamidi, H., Mohammadian, E., Honarvar, B., (2018), "CO_2 sequestration through direct aqueous mineral carbonation of red gypsum", Petroleum, 4, 398-407, doi.org/10.1016/j.petlm.2017.10.002.

[107] Santos, T., Gomes, M.I., Silva, A.S., Ferraz, E., Faria, P., (2020), "Comparison of mineralogical, mechanical and hygroscopic characteristic of earthen, gypsum and cement-based plasters", Construction and Building Materials, Construction and Building Materials, 254, 119222, doi.org/10.1016/j.conbuildmat.2020.119222.

[108] Essabir, H., Raji, M., Nekhlaoui, S., Hassani, I.A., Essassi, M., Rodrigue, D., Bouhfid, R., Qaiss, A., (2019), "Utilization of volcanic amorphous aluminosilicate rocks (perlite) as alternative materials in lightweight composites", Composites Part B, 165, 47-54, doi.org/10.1016/j.compositesb.2018.11.098.

[109] Mucahit, S., (2014), "Influence of expanded vermiculite on physical properties and thermal conductivity of clay bricks", Ceramics International, 41, 2819-2827, doi.org/10.1016/j.ceramint.2014.10.102.

[110] Cabuk, M., Yesil, T.A., Yavuz, M., Unal, H.I., (2017), "Colloidal and viscoelastic properties of expanded perlite dispersions", Journal of Intelligent Material Systems and

Structures, doi:10.1177/1045389X17698248.

[111] Wang, Z., Xia, Z., (2019), "Rigid polyurethane/expanded vermiculite/ melamine phenylphosphate composite foams with good flame retardant and mechanical properties", e-Polymers, 19, 563–573, doi.org/10.1515/epoly-2019-0060.

[112] Mahmoud, M.H.H, Rashad, M.M., Ibrahim, I.A., Abdel-Aal, E.A., (2003), "Crystal modification of calcium sulfate dihydrate in the presence of some surface-active agents", Journal of Colloid and Interface Science, 270, 99–105, doi:10.1016/j.jcis.2003.09.023.

[113] Feng, Q., Deng, Y., Kim, H., Lei, W., Sun, Z., Jia, Y., Xuan, L., Kim, S., (2006), "Observation and Analysis of Gypsum Particleboard using SEM", Journal of Wuhan University of Technology-Materials Sciences, Vol. 22 No.1, doi:10.1007/s11595-005-1044-z.

[114] Oliveira, M., (2022), "Study of the degradation of 18th century alabaster sculptures through accelerated ageing on test samples", doi.org/10.4000/ceroart.3187.

[115] Chu, D.C., Kleib, J., Amar, M., Benzerzour, M., Abriak, N., (2021), "Determination of the degree of hydration of Portland cement using three different approaches: Scanning electron microscopy (SEM-BSE) and Thermogravimetric analysis (TGA)", Case Studies in Construction Materials, 15, e00754, doi.org/10.1016/j.cscm.2021.e00754.

[116] Roßler, C., Zimmer, D., Trimby, P., Ludwig, H., (2022), "Chemical – crystallographic characterisation of cement clinkers by EBSD-EDS analysis in the SEM", Cement and Concrete Research, 154, 106721, doi.org/10.1016/j.cemconres.2022.106721.

[117] Wang, K., Sargam, Y., (2021), "Quantifying dispersion of nanosilica in hardened cement matrix using a novel SEM-EDS and image analysis-based methodology", Cement and Concrete Research, 147, 106524, doi.org/10.1016/j.cemconres.2021.106524.

[118] Lim, S., Lee, H., Kawashima, S., (2018), "Pore structure refinement of cement paste incorporating nanosilica: Study with dual beam scanning electron microscopy/focused ion beam (SEM/FIB)", Materials Characterization, 145, 323-328, doi.org/10.1016/j.matchar.2018.08.045.

[119] Gercek, H., (2006), "Poisson's ratio values for rocks", International Journal of Rock Mechanics & Mining Sciences, 44, 1–13, doi.10.1016/j.ijrmms.2006.04.011.

[120] Mayo-Corrochano, C., Sánchez-Aparicio, L.J., Aira, J, Sanz-Arauz, D., Moreno, E., Melo, J.P., (2021), "Assessment of the elastic properties of high-fired gypsum using the digital image correlation method", Construction and Building Materials, doi.org/10.1016/j.conbuildmat.2021.125945.

[121] Nettleton, D.F., (2014), "Selection of Variables and Factor Derivation", Chapter 6 79-104, Commercial Data Mining, doi.org/10.1016/B978-0-12-416602-8.00006-6.

[122] Babu, K.S., Ratnam, Ch., (2021), "Mechanical and thermophysical behaviour of hemp fibre reinforced gypsum composites", Materials Today: Proceedings, 44, 2245–2249, doi.org/10.1016/j.matpr.2020.12.363.

[123] Vegas, F., Mileto, C., Ivorra, S., Baeza, F.J., (2012), "Checking Gypsum as Structural Material", Applied Mechanics and Materials, Vols. 117-119, 1576-1579,

doi.org/10.4028/www.scientific.net/AMM.117-119.1576.

[124] EN 13279-1, (2005), "Gypsum binders and gypsum plasters. Part 1: Definitions and requirements".

[125] Koksal, F., Nazli, T., Benli, A., Gencel, O., Kaplan, G., (2021), "The effects of cement type and expanded vermiculite powder on the thermo- mechanical characteristics and durability of lightweight mortars at high temperature and RSM modelling", Case Studies in Construction Materials, 15, e00709, doi.org/10.1016/j.cscm.2021.e00709.

[126] Summers, H.B., (1932), "A Comparison of the Rates of Earning of Large-Scale and Small-Scale Industries", The Quarterly Journal of Economics, Vol. 46, No. 3, 465-479, Oxford Journals

[127] Bernesson, S., Nilsson, D., Hanssom, P., (2006), "A limited LCA comparing large- and small-scale production of ethanol for heavy engines under Swedish conditions", Biomass and Bioenergy, 30, 46-47, doi.10.1016/j.biombioe.2005.10.002.

APPENDIX A – NON-DESTRUCTIVE TESTS

Appendix A shows, in section A1, the photos of the intact specimens before the tests and, in section A2, it is possible to see the dynamic modulus of elasticity, the shear modulus and the Poisson's ratio results for each specimen.

A.1 Photos of the specimens before the tests

Table A.1 – Photos of each specimen before the tests

C composition			
			
C.1	**C.2**	**C.3**	**C.4**
CV composition			
			
CV.1	**CV.2**	**CV.3**	**CV.4**
CV.NMS composition			
			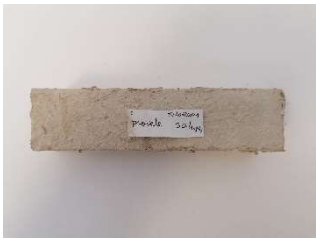
CV.NMS.1	**CV.NMS.2**	**CV.NMS.3**	**CV.NMS.4**

GP composition

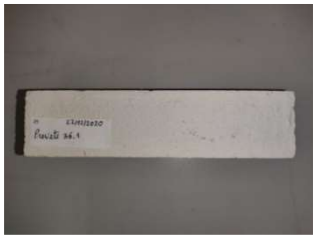

GP.1

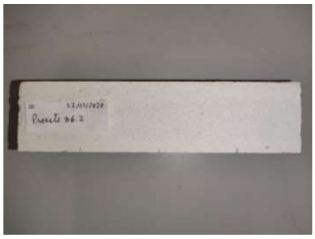

GP.2

GP.3

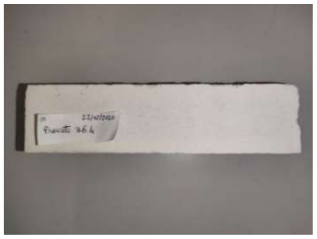

GP.4

GP.NMS composition

GP.NMS.1

GP.NMS.2

GP.NMS.3

GP.NMS.4

GV composition

GV.1

GV.2

GV.3

GV.4

GV.NMS composition

GV.NMS.1

GV.NMS.2

GV.NMS.3

GV.NMS.4

A.2 Non-destructive tests' results

Table A.2 – Non-destructive tests' results for each specimen.

Mortar Designation	E (GPa)		G (GPa)		μ	
	UPV test	IEV test	UPV test	IEV test	UPV test	IEV test
C.1	2.656	2.601	1.130	1.091	0.18	0.19
C.2	2.656	2.601	1.130	1.091	0.18	0.19
C.3	2.656	2.601	1.130	1.091	0.18	0.19
C.4	2.656	2.601	1.130	1.091	0.18	0.19
CV.1	0.772	0.765	0.294	0.289	0.32	0.32
CV.2	0.772	0.765	0.294	0.289	0.32	0.32
CV.3	0.772	0.765	0.294	0.289	0.32	0.32
CV.4	0.772	0.765	0.294	0.289	0.32	0.32
CV.NMS.1	0.933	0.921	0.350	0.347	0.33	0.33
CV.NMS.2	0.933	0.921	0.350	0.347	0.33	0.33
CV.NMS.3	0.933	0.921	0.350	0.347	0.33	0.33
CV.NMS.4	0.933	0.921	0.350	0.347	0.33	0.33
GP.1	1.070	1.381	0.412	0.564	0.30	0.22
GP.2	1.181	1.381	0.472	0.564	0.25	0.22
GP.3	1.136	1.381	0.446	0.564	0.27	0.22
GP.4	0.913	1.381	0.374	0.564	0.22	0.22
GP.NMS.1	1.212	1.293	0.491	0.533	0.23	0.21
GP.NMS.2	1.212	1.293	0.491	0.533	0.23	0.21
GP.NMS.3	1.212	1.293	0.491	0.533	0.23	0.21
GP.NMS.4	1.212	1.293	0.491	0.533	0.23	0.21
GV.1	3.175	2.721	1.370	1.111	0.16	0.22
GV.2	2.537	2.721	0.979	1.111	0.29	0.22
GV.3	3.028	2.721	1.301	1.111	0.16	0.22
GV.4	2.411	2.721	0.915	1.111	0.32	0.22
GV.NMS.1	2.674	2.708	1.116	1.118	0.20	0.21
GV.NMS.2	2.674	2.708	1.116	1.118	0.20	0.21
GV.NMS.3	2.674	2.708	1.116	1.118	0.20	0.21
GV.NMS.4	2.674	2.708	1.116	1.118	0.20	0.21

APPENDIX B – FLEXURAL TEST

Appendix B is shown, in section B1, the photos of the specimens after the flexural tests. In section B2, it is possible to observe the load-displacement curves of the flexural tests and, in section B3, the flexural strength results for each specimen.

B.1 Photos of the specimens after the flexural tests

Table B.1 – Specimen's photos after the flexural test.

C.1	**C.2**
	
C.3	**C.4**
	
CV.1	**CV.2**
	
CV.3	**CV.4**
	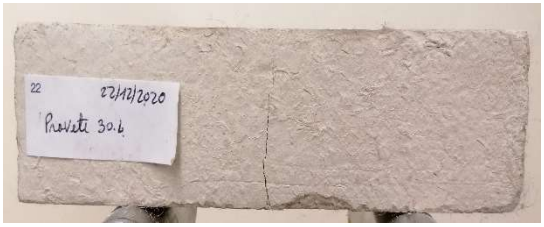
CV.NMS.1	**CV.NMS.2**

CV.NMS.3

CV.NMS.4

GP.1

GP.2

GP.3

GP.4

GP.NMS.1

GP.NMS.2

GP.NMS.3

GP.NMS.4

GV.1

GV.2

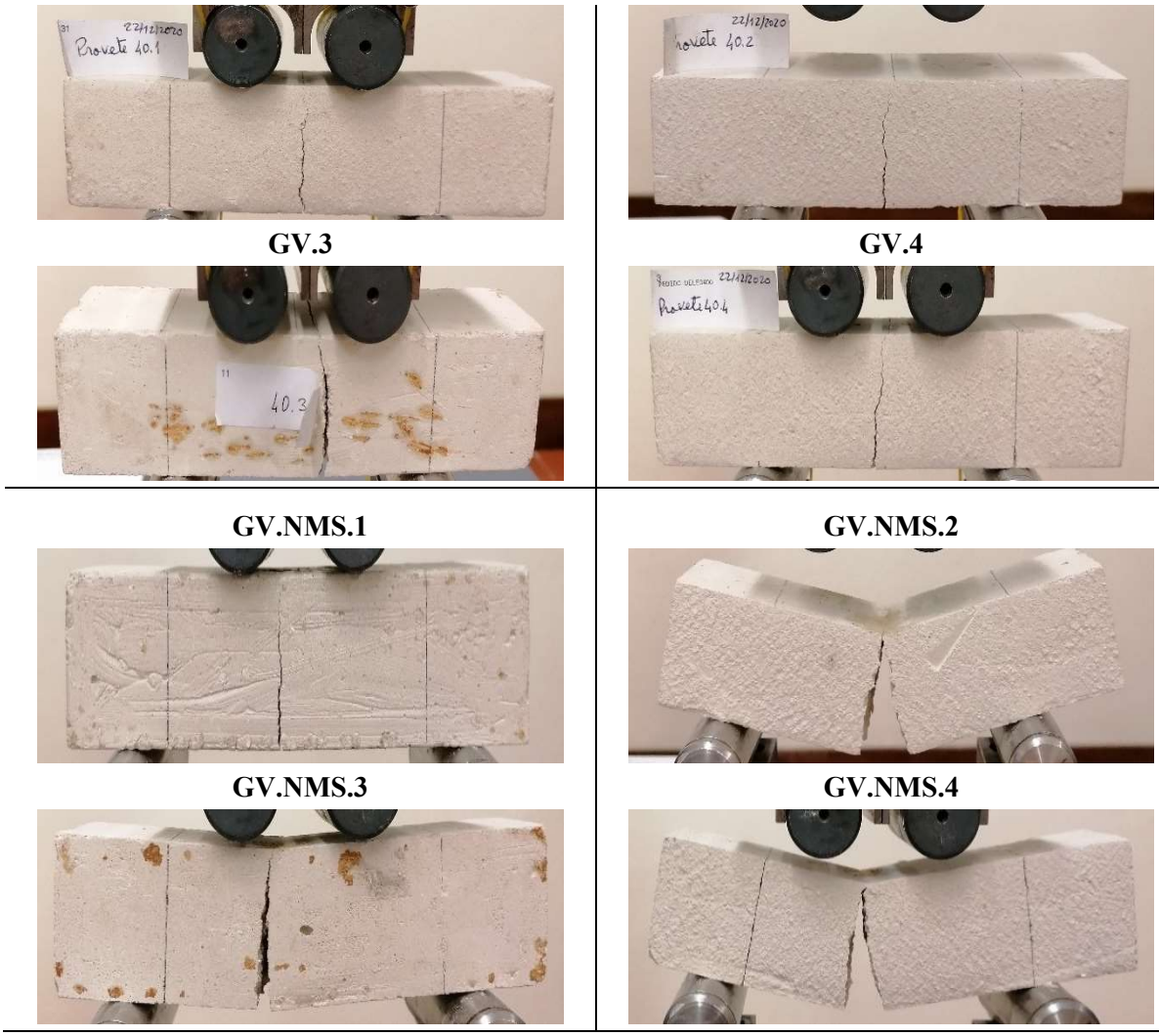

B.2 Load-displacement curves results

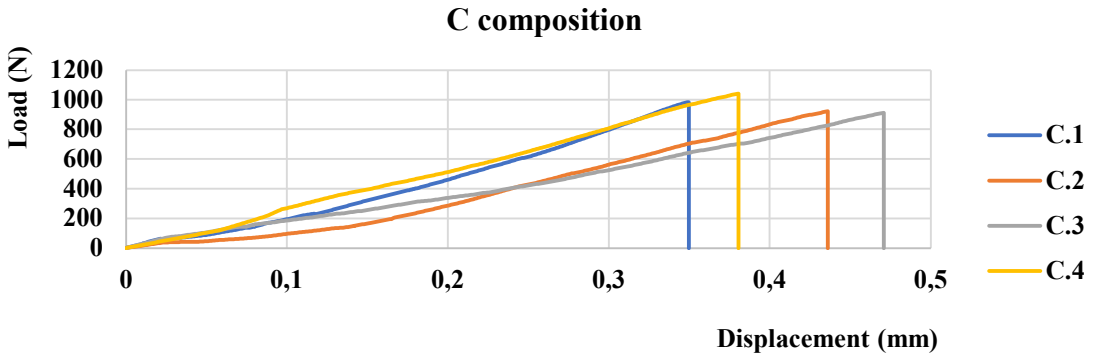

Figure B.1 – C composition's load – displacement curves of each specimen.

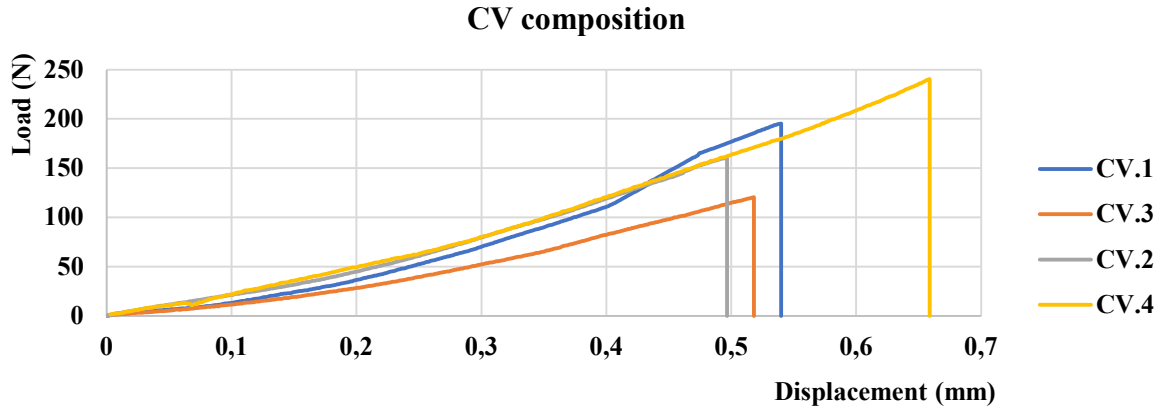

Figure B.2 – CV composition's load – displacement curves of each specimen

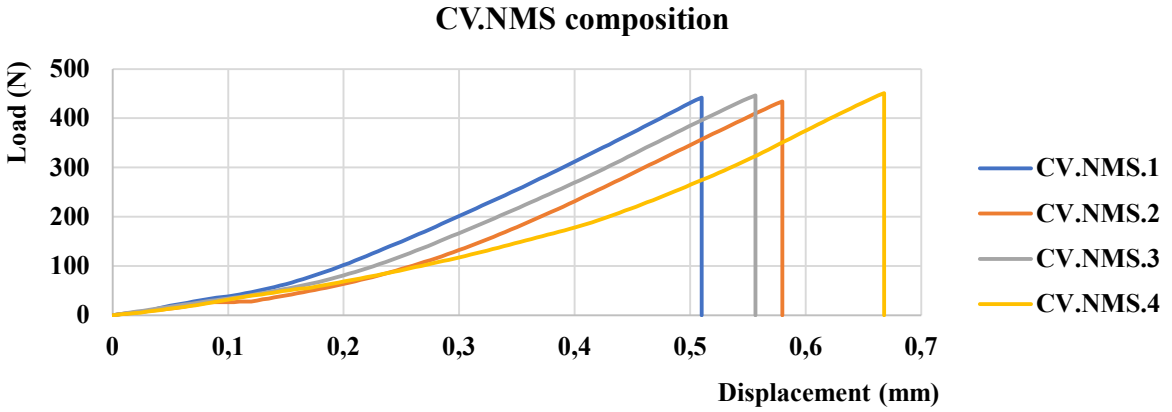

Figure B.3 – CV.NMS composition's load – displacement curves of each specimen

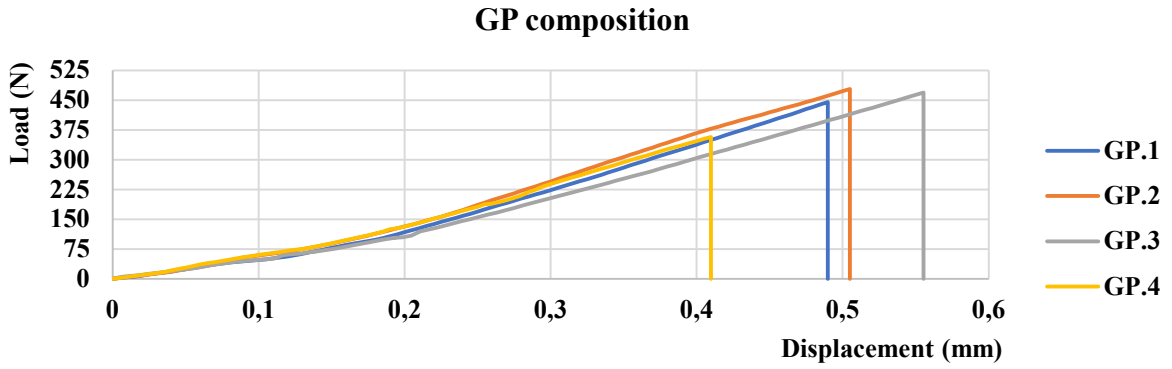

Figure B.4 - GP composition's load – displacement curves of each specimen.

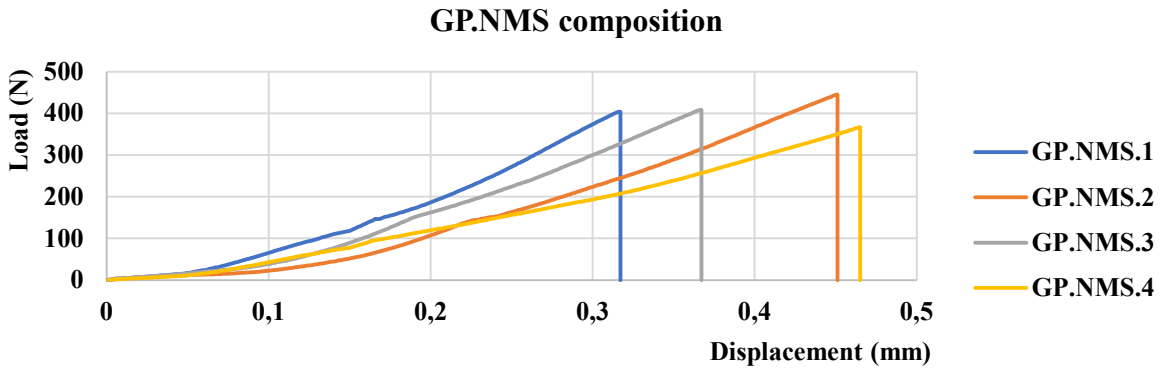

Figure B.5 - GP.NMS composition's load – displacement curves of each specimen.

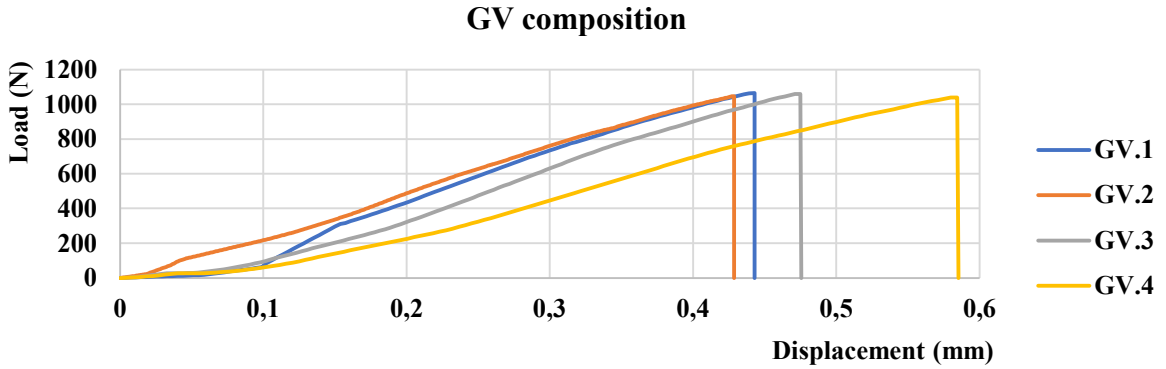

Figure B.6 - GV composition's load – displacement curves of each specimen.

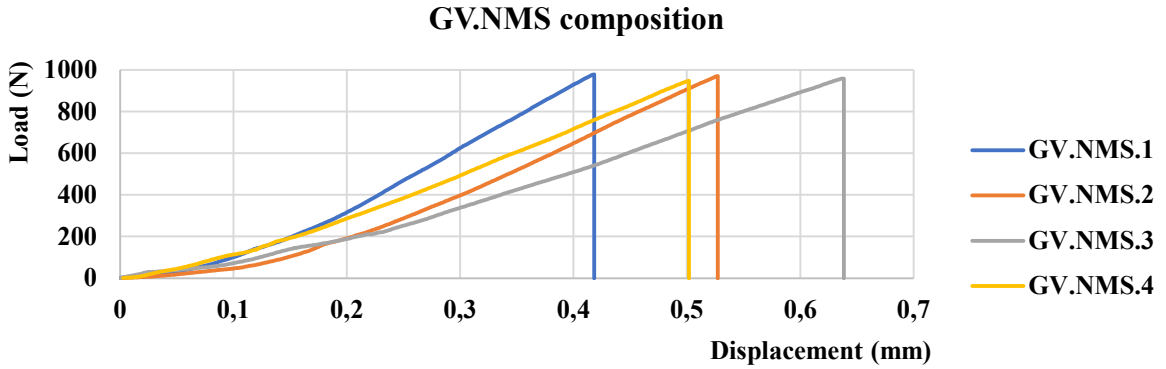

Figure B.7 - GV.NMS composition's load – displacement curves of each specimen.

B.3 Flexural strength's results

Table B.2 - Flexural strength's results for each specimen.

Specimen Designation	Maximum Load (N)	Flexural Strength (MPa)
C.1	984.0	2.037
C.2	922.9	1.910
C.3	911.3	1.886
C.4	1041.3	2.156
CV.1	195.3	0.404
CV.2	160.2	0.332
CV.3	120.6	0.250
CV.4	240.5	0.498
CV.NMS.1	442.0	0.915
CV.NMS.2	434.6	0.900
CV.NMS.3	446.9	0.925
CV.NMS.4	451.5	0.935
GP.1	445.4	0.922
GP.2	478.1	0.990
GP.3	460.4	0.953
GP.4	357.4	0.740
GP.NMS.1	404.1	0.836
GP.NMS.2	445.6	0.922
GP.NMS.3	408.9	0.847
GP.NMS.4	366.8	0.759
GV.1	1065.4	2.205
GV.2	1047.7	2.169
GV.3	1059.3	2.193
GV.4	1039.1	2.151
GV.NMS.1	979.1	2.027
GV.NMS.2	971.4	2.011
GV.NMS.3	959.0	1.985
GV.NMS.4	947.6	1.962

APPENDIX C – COMPRESSION TEST

Appendix C is shown, in section C1, the photos of the specimens after the compression tests. In section C2, it is possible to observe the load-displacement curves of the compression tests and, in section C3, the compression strength results for each specimen.

C.1 Photos of the specimens after the compression tests

Table C.1 – Specimen's photos after the compression test.

CV.1.1	**CV.1.2**
	
CV.2.1	**CV.2.2**
	
CV.3.1	**CV.3.2**
	
CV.4.1	**CV.4.2**
	
CV.NMS.1.1	**CV.NMS.1.2**

*** No photo registered.**

CV.NMS.2.1

*** No photo registered.**

*** No photo registered.**

CV.NMS.2.2

*** No photo registered.**

CV.NMS.3.1

CV.NMS.3.2

CV.NMS.4.1

CV.NMS.4.2

GP.1.1

GP.1.2

GP.2.1

GP.2.2

GP.3.1

GP.3.2

GP.4.1

GP.4.2

GP.NMS.1.1

GP.NMS.1.2

GP.NMS.2.1

GP.NMS.2.2

GP.NMS.3.1

GP.NMS.3.2

GP.NMS.4.1

GP.NMS.4.2

GV.1.1

GV.1.2

GV.2.1

GV.2.2

GV.3.1

GV.3.2

GV.4.1

GV.4.2

GV.NMS.1.1

GV.NMS.1.2

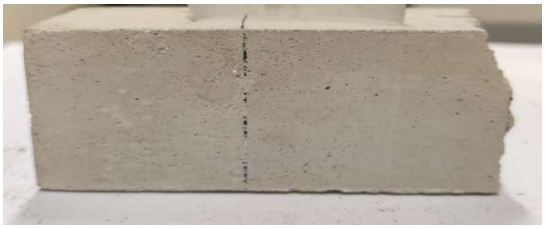

GV.NMS.2.1

GV.NMS.2.2

GV.NMS.3.1

GV.NMS.3.2

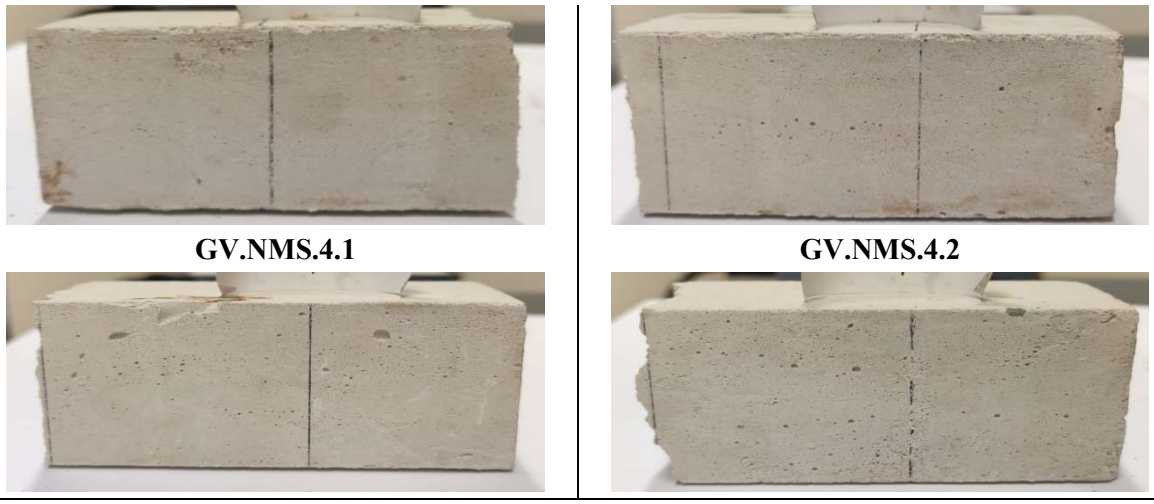

* The commercial solution's compression tests' photos weren't registered.

C.2 Load-displacement curves results

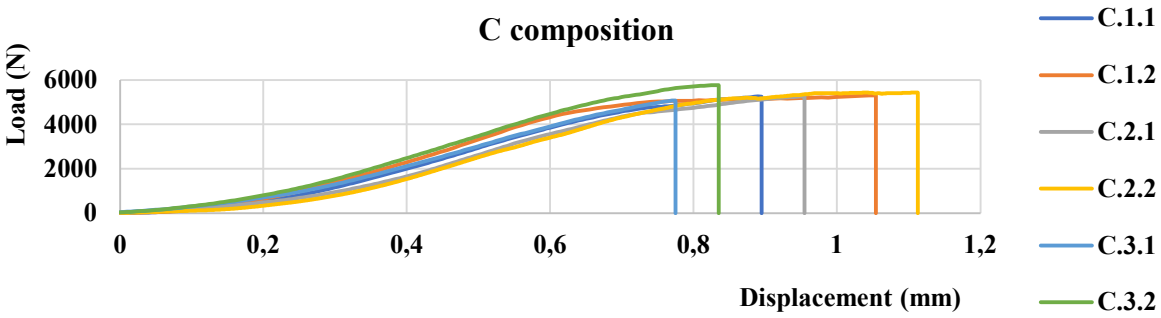

Figure C.1 – C composition's load – displacement curves of each specimen.
* C.4.1 and C.4.2 have no data due to machine's error.

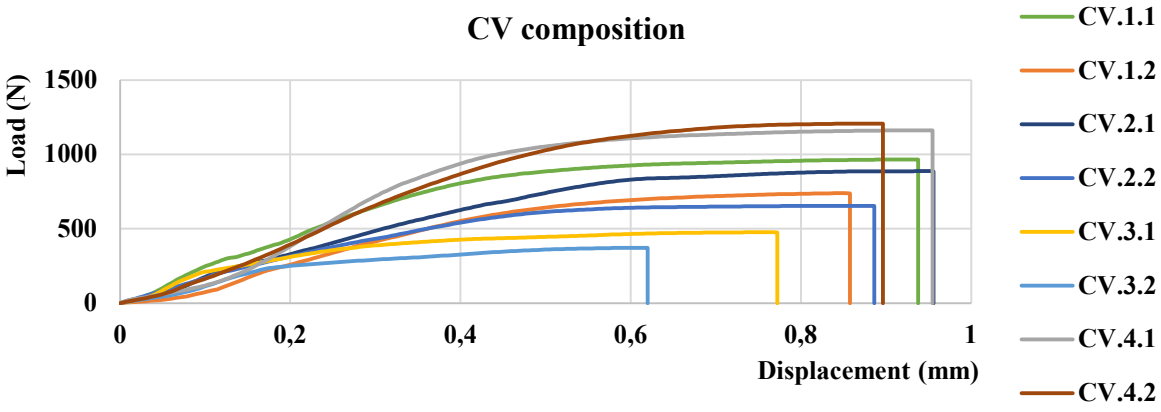

Figure C.2 - CV composition's load – displacement curves of each specimen.

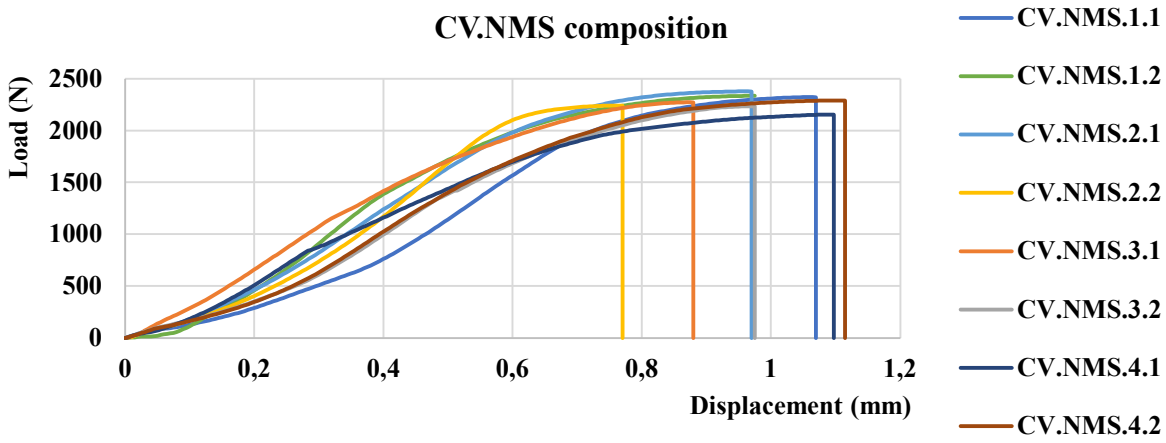

Figure C.3 – CV.NMS composition's load – displacement curves of each specimen.

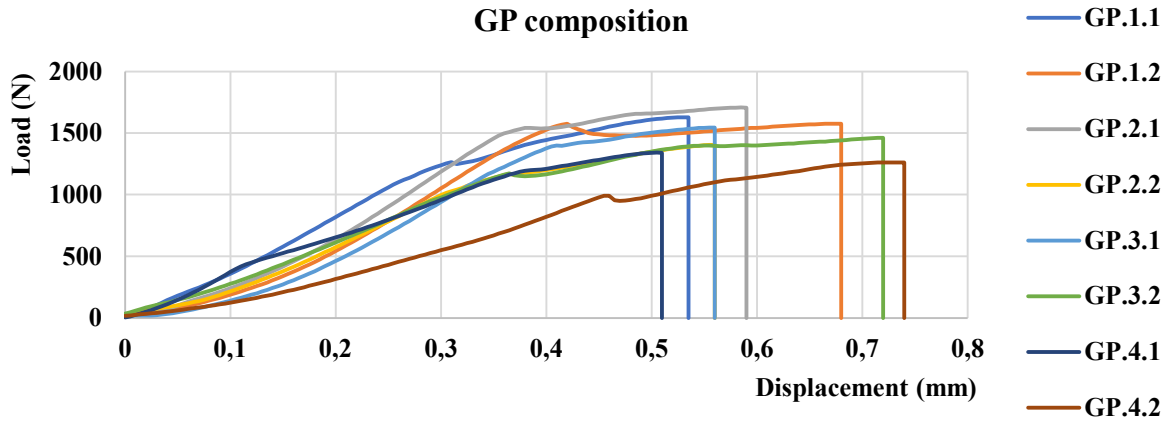

Figure C.4 – GP composition's load – displacement curves of each specimen.

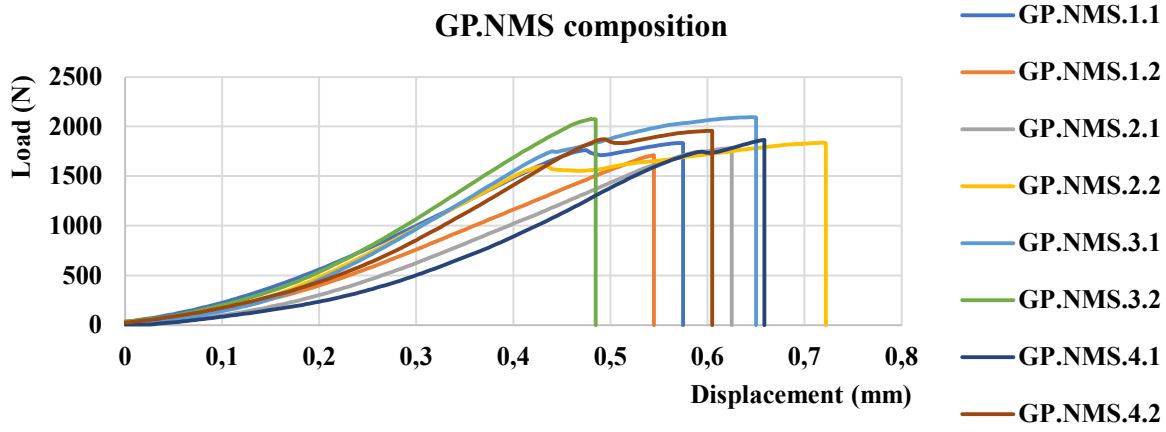

Figure C.5 – GP.NMS composition's load – displacement curves of each specimen.

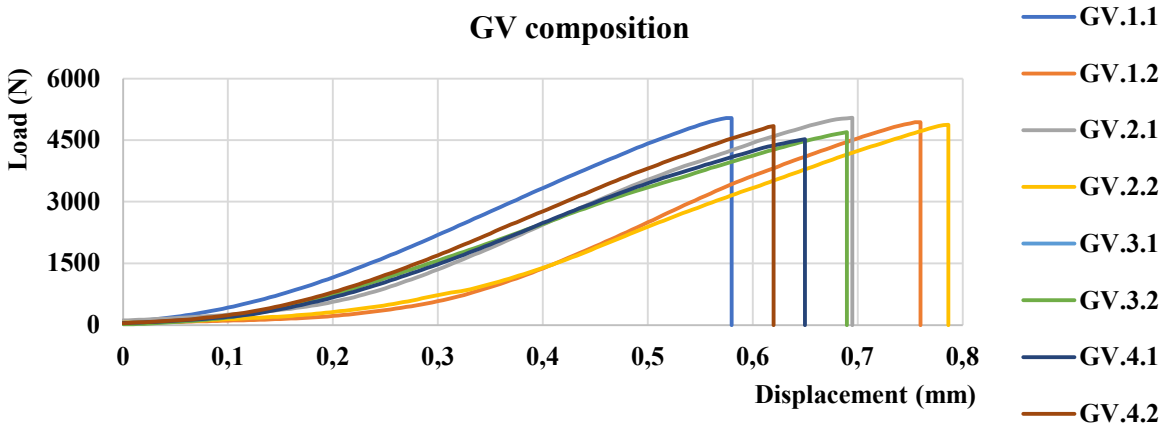

Figure C.6 – GV composition's load – displacement curves of each specimen.

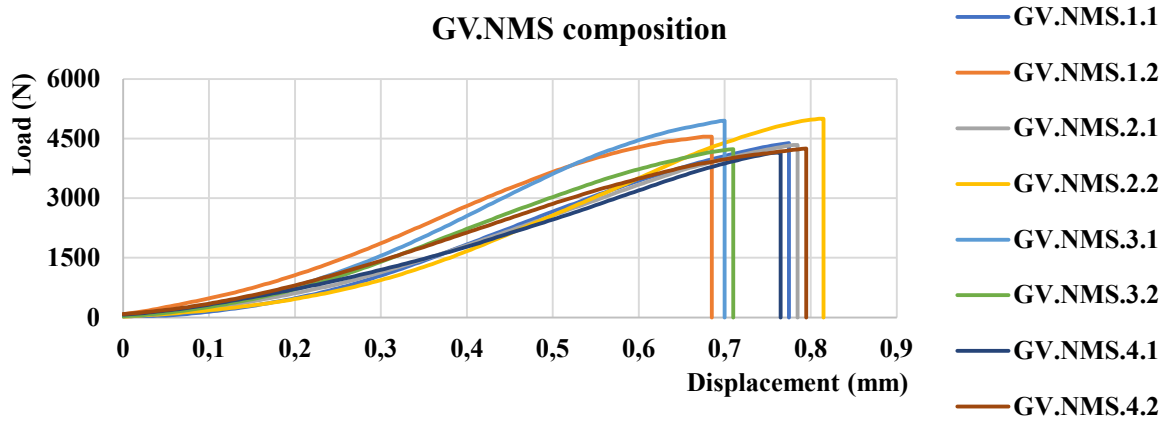

Figure C.7 – GV.NMS composition's load – displacement curves of each specimen.

C.3 Compression strength's results

Table C.2 – Compression strength's results for each specimen.

Specimen Designation	Maximum Load (N)	Compression Strength (MPa)
C.1.1	5259.0	3.287
C.1.2	5306.1	3.316
C.2.1	5260.5	3.288
C.2.2	5439.9	3.400
C.3.1	5078.9	3.174
C.3.2	5766.4	3.604
C.4.1	-	-
C.4.2	-	-
CV.1.1	965.5	0.603
CV.1.2	738.5	0.462
CV.2.1	886.5	0.554

CV.2.2	653.9	0.409
CV.3.1	476.3	0.298
CV.3.2	371.8	0.232
CV.4.1	1160.8	0.726
CV.4.2	1205.8	0.754
CV.NMS.1.1	2322.6	1.452
CV.NMS.1.2	2335.3	1.460
CV.NMS.2.1	2378.2	1.486
CV.NMS.2.2	2241.0	1.410
CV.NMS.3.1	2272.5	1.420
CV.NMS.3.2	2234.6	1.397
CV.NMS.4.1	2154.2	1.346
CV.NMS.4.2	2289.6	1.431
GP.1.1	1628.0	1.017
GP.1.2	1575.4	0.985
GP.2.1	1706.4	1.066
GP.2.2	1404.6	0.878
GP.3.1	1544.3	0.965
GP.3.2	1462.1	0.914
GP.4.1	1340.5	0.838
GP.4.2	1261.5	0.788
GP.NMS.1.1	1833.9	1.146
GP.NMS.1.2	1711.7	1.070
GP.NMS.2.1	1782.1	1.114
GP.NMS.2.2	1835.7	1.147
GP.NMS.3.1	2093.2	1.308
GP.NMS.3.2	2074.4	1.297
GP.NMS.4.1	1865.4	1.166
GP.NMS.4.2	1957.1	1.223
GV.1.1	5040.3	3.150
GV.1.2	4937.9	3.086
GV.2.1	5044.3	3.153
GV.2.2	4873.1	3.046
GV.3.1	4522.2	2.845
GV.3.2	4694.8	2.934
GV.4.1	4522.5	2.827
GV.4.2	4846.3	3.029
GV.NMS.1.1	4387.8	2.742
GV.NMS.1.2	4552.8	2.845
GV.NMS.2.1	4341.9	2.714
GV.NMS.2.2	5001.0	3.126
GV.NMS.3.1	4953.3	3.096
GV.NMS.3.2	4238.4	2.649
GV.NMS.4.1	4148.9	2.593
GV.NMS.4.2	4253.3	2.658